THESIS ON CHEMISTRY AND CHEMICAL ENGINEERING G31

Gas-Phase Photocatalytic Oxidation of Organic Air Pollutants

SVETLANA JÕKS

TUT PRESS

TALLINN UNIVERSITY OF TECHNOLOGY
Faculty of Chemical and Materials Technology
Department of Chemical Engineering

Dissertation was accepted for the defence of the degree of Doctor of Philosophy in Engineering on March 29, 2012

Supervisor: Senior Research Scientist Dr. Marina Kritševskaja, Department of Chemical Engineering, Tallinn University of Technology

Opponents: Dr. Gundula Helsch, Clausthal University of Technology, Germany

Dr. Ekaterina A. Kozlova, Boreskov Institute of Catalysis SB RAS, Russia

Defence of the thesis: May 29, 2012, 11:00
Lecture Hall VII-226
Tallinn University of Technology, Ehitajate tee 5, Tallinn

Declaration:
Hereby I declare that this doctoral thesis, my original investigation and achievement, submitted for the doctoral degree at Tallinn University of Technology has not been submitted for any academic degree.

Svetlana Jõks

This work has been partially supported by graduate school "Functional materials and technologies" receiving funding from the European Social Fund under project 1.2.0401.09-0079 in Estonia."

Copyright: Svetlana Jõks, 2012
ISSN: 1406-4774
ISBN: 978-9949-23-266-6 (publication)
ISBN: 978-9949-23-267-3 (PDF)

KEEMIA JA KEEMIATEHNIKA G31

Orgaaniliste õhu saasteainete fotokatalüütiline oksüdatsioon gaasifaasis

SVETLANA JÕKS

TTÜ
KIRJASTUS

TABLE OF CONTENTS

TABLE OF CONTENTS 5
LIST OF PUBLICATIONS 6
THE AUTHOR'S CONTRIBUTION TO PUBLICATIONS 7
LIST OF ABBREVIATIONS, TERMS AND SYMBOLS 8
INTRODUCTION 9
ACKNOWLEDGMENTS 10
1. LITERATURE REVIEW 11
    1.1 Photocatalytic oxidation on titanium dioxide 11
    1.2 Flame aerosol synthesis of titanium dioxide 14
    1.3 Sulphation of titanium dioxide 14
    1.4 Effect of humidity and temperature on the performance of gas-phase photocatalytic oxidation 15
    1.5 Objectives and strategies of the study 17
2. MATERIALS AND METHODS 17
    2.1 Continuous-flow mode 18
    2.2 Transient mode 20
    2.3 Preparation of TiO_2 coatings 22
3. RESULTS AND DISCUSSION 23
    3.1 Products of acrylonitrile photocatalytic and thermal oxidation 23
    3.2 Effect of process parameters on gas-phase photocatalytic oxidation of acrylonitrile 24
    3.3 Photocatalytic oxidation of acrylonitrile over sulphated P25 photocatalyst 26
    3.4 Photocatalytic oxidation of acrylonitrile and toluene over flame synthesized F3 photocatalyst 27
CONCLUSIONS 28
REFERENCES 30
ABSTRACT 38
KOKKUVÕTE 39
APPENDIX I. PUBLICATIONS 41
    PAPER I 43
    PAPER II 49
    PAPER III 59
APPENDIX II. CURRICULUM VITAE 71

LIST OF PUBLICATIONS

I. Krichevskaya, M., Jõks, S., Kachina, A., Preis, S. 2009. Gas-phase photocatalytic oxidation of acrylonitrile. - Photochemical and Photobiological Sciences, 8(5), p. 600 - 603.

II. Jõks, S., Krichevskaya, M., Preis, S. 2011. Gas-phase photocatalytic oxidation of acrylonitrile on sulphated TiO_2: continuous flow and transient study. - Catalysis Letters, 141(2), p. 309 - 315.

III. Jõks, S., Klauson, D., Krichevskaya, M., Preis, S., Qi, F., Weber, A., Moiseev, A., Deubener, J. 2012. Gas-phase photocatalytic activity of nanostructured titanium dioxide from flame aerosol synthesis. - Applied Catalysis B: Environmental, 111-112, p. 1 - 9.

Other publications:

Krichevskaya, M., Jõks, S., Kachina, A., Preis, S. 2008. Gas-phase photocatalytic oxidation of acrylonitrile. - Book of Abstracts: The 5th European Meeting on Solar Chemistry and Photocatalysis: Environmental Applications (SPEA5), 04-08 October 2008, Palermo, Italy, PP2.20.

Jõks, S., Kritševskaja, M., Preis, S. 2010. Akrüülnitriili fotokatalüütiline oksüdatsioon gaasifaasis. - Teaduskonverentsi teesid: XXXI Eesti Keemiapäevad, 28 April 2010, Tallinn, Estonia.

Jõks, S., Klauson, D., Krichevskaya, M., Preis, S., Moiseev, A., Qi, F., Deubener, J., Weber, A. 2011. Gas-phase photocatalytic activity of nanostructured titanium dioxide from diffusion flame synthesis. - Book of Abstracts: Photocatalytic and Advanced Oxidation Technologies for Treatment of Water, Air, Soil and surfaces (PAOT 2011), 04-08 July 2011, Gdansk, Poland, p 62.

THE AUTHOR'S CONTRIBUTION TO PUBLICATIONS

The contribution of the author of present thesis to the papers listed above is as follows:

I. The author carried out a major part of the experimental work, and participated in data processing and in the discussion of the results.

II. The author carried out a major part of the experimental work, participated in processing and discussion of the results, contributing the major part of writing.

III. The author carried out the experimental work, participated in data processing and in the discussion of the results. The paper was written by the author together with the co-authors.

LIST OF ABBREVIATIONS, TERMS AND SYMBOLS

4-CP	4-chlorophenol
AN	acrylonitrile
C	concentration of volatile organic compound
CB	conduction band
C_{in}	inlet concentration
C_{out}	outlet concentration
DCA	dichloroacetic acid
DNA	deoxyribonucleic acid
EPA	Environmental Protection Agency
FT-IR	Fourier transform infrared
LUT	Lappeenranta University of Technology
PCO	photocatalytic oxidation
ppm	parts per million
ppmv	parts per million by volume
R	polluting species
RH	relative humidity
T	temperature
t	time
TCE	trichloroethylene
TPO	temperature-programmed oxidation
TUT	Tallinn University of Technology
USA	United States of America
UV	ultraviolet
VB	valence band
VOC	volatile organic compound
WHO	World Health Organization

INTRODUCTION

Both indoor and outdoor air quality has become an important community concern due to ubiquitous presence of air pollutants like carbon, nitrogen and sulphur oxides, particulates and volatile organic compounds (VOCs). The increased amount of personnel time spent in indoor environment makes the science confront the VOCs as the most abundant chemical pollutants in the indoor air. Some studies showed that the level of pollutants in indoor environment actually exceeds that of the outdoors (Wang et al., 2007). VOCs are emitted from building materials, office equipment, cleaning agents, paints, glues, solvents, cosmetics, cooking and most manufactured consumer products. Many VOCs are known to be toxic and considered to be carcinogenic (WHO, 2010). Therefore, there is currently a great interest in developing processes which can destroy these compounds. Air cleaning is the most feasible option to improve air quality as the source control is often ungovernable.

Traditionally filters and sorbents are used to remove particulates and odours. However, the contaminants are only transferred to another phase rather than eliminated by these techniques and subsequent disposal or treatment steps are required.

Since a large number of the VOCs are oxidizable, oxidation process can be a viable method. Thermal catalytic oxidation requires high temperatures (250-1200 °C) and as high as hundreds of ppm concentrations of VOCs for successful operation being cost-ineffective for low pollutant concentrations (Van der Vaart et al., 1991; Gervasini and Ragaini, 2000; Hung and Chu, 2006). Photocatalytic oxidation (PCO) technique is of extensive interest recently as potential air-cleaning technology for lower VOCs concentrations and indoor applications (Zhao and Yang, 2003; Paz, 2010). Photocatalytic processes based on the absorption of near UV radiation by the semiconductor photocatalyst with further oxidation of organic molecules possess certain advantages such as (a) complete mineralisation of organic pollutants achieved under favourable conditions, (b) efficiency at ambient temperature and pressure, and (c) cost-effective character as compared to other conventional techniques.

Hazardous air pollutants, aliphatic heteroatomic acrylonitrile (AN) and aromatic hydrophobic toluene were chosen for gas-phase PCO studies. Both of them are included to the Environmental Protection Agency (EPA) list of hazardous air pollutants. Acrylonitrile is detected as an indoor air component emitted by commercial fibrous polymeric materials, resins and smoking tobacco (Byrd et al., 1990; Scherer et al., 2007); it can induce gene mutations, chromosome aberrations, unscheduled DNA synthesis and cell transformation (Léonard et al., 1999). Toluene is used in motor fuel octane ratings improvement, in the synthesis of various organic chemicals and pharmaceuticals, in the production

of polymers and as a solvent in paints, coatings, synthetic fragrances, adhesives, inks and cleaning agents (EPA, 1999). The central nervous system, kidneys, liver and heart are the primary targets for toluene toxicity (ATSDR, 1994).

The PCO of toluene using commercial TiO_2 catalysts has been extensively studied (Méndez-Román and Cardona-Martínez, 1998; Augugliaro, et al., 1999; Piera et al., 2002; Belver et al., 2003; Mo et al., 2009). Toluene presents serious problem in the long-term photocatalyst activity exhibiting pronounced deactivation properties (Obee and Brown, 1995; Paz, 2010). The abundance in published data allows toluene being a reference pollutant in characterization of the catalysts and, in general, the abatement methods.

The wide diversity of organic pollutants decomposed by PCO at the UV-irradiated TiO_2 surface justifies the experimental research into the photocatalytic degradation of chosen pollutants together with the search for more active photocatalytic materials.

ACKNOWLEDGMENTS

The author is deeply indebted to the supervisor of her thesis Dr. Marina Krichevskaya for introducing her into the field of photocatalytic oxidation and for giving her the necessary knowledge about chemical engineering. Her invaluable support, friendship and advices were extremely helpful and essential during all five years of collaboration.

The special appreciation belongs to Dr. Sergei Preis for his valuable advices during the research. Dr. Preis and Prof. John L. Falconer granted the opportunity to carry out the transient study experiments at the University of Colorado, Boulder, USA, supported by the joint US-Estonian research project.

The author would like to express sincere gratitude to Dr. Deniss Klauson for the contribution to the discussions. Special thanks go to Dr. Anna Moiseev for the fruitful collaboration and helpful remarks and to Dr. Anna Kachina for the performing FT-IR analysis at Lappeenranta University of Technology, Finland, and sharing her experience.

Also, I would like to sincerely thank all my family, friends and work colleagues for supporting me during this period and providing the pleasant working atmosphere.

Financial support from Estonian Science Foundation and Ministry of Education and Research (grants 7541, 8978, GUS16062, GUS10 and SF0140022s10), United States Civilian Research and Development Foundation (grants ESE2-2899-TL-07 and ESC2-2974-TL-09), The Estonian Doctoral School of „Functional materials and technologies" (FMTDK) is gratefully acknowledged.

1. LITERATURE REVIEW

1.1 Photocatalytic oxidation on titanium dioxide

Studies of TiO_2 photoactivity have been reported firstly by Fujishima and Honda in 1972, while carrying out experiments on the photo-oxidation of water on TiO_2 electrodes (Fujishima and Honda, 1972). Heterogeneous photocatalysis is the catalytic process during which one or more reaction steps occur by means of electron–hole pair photogenerated on the surface of semiconducting materials illuminated by light of suitable energy (Palmisano and Sclafani, 1997).

Being extensively studied in early 1990s, photocatalysis was mainly applied to aqueous solutions. The gas-phase photocatalysis using TiO_2 was initially explored by Dibble and Raupp (1990), and the interest to the gas-phase photocatalytic oxidation has been constantly increasing during the past years (Paz, 2010). The promising areas of the photocatalysis application are the removal of organic and inorganic pollutants (Ollis, 2000; Mo et al., 2009; Shivaraju, 2011; Zhong and Haghighat, 2011), selective synthesis of organic compounds (Shiraishi and Hirai, 2008; Siham and Hussein, 2009; Hoffmann et al., 2011), microbial contamination control (Kozlova et al., 2010; Gamage and Zhang, 2011; Foster et al., 2011) and self-cleaning and anti-fogging materials (Zhao et al., 2008; Fujishima et al., 2008; Chen et al., 2011).

The most important step of PCO is the formation of hole–electron pairs, which need energy to overcome the band gap between the valence band and conduction band. When photons have a higher energy, than this band gap, they can be absorbed and an electron is promoted to the conduction band, leaving a hole in the valence band (Wang, 2004). Several semiconductors have band gap energies sufficient for promoting or catalyzing a wide range of chemical reactions of environmental interest (Lin, 2008). Among many candidates, titanium dioxide has proven to be the most suitable for widespread environmental applications because of its biological and chemical inertness, stability against photo corrosion and chemical corrosion, and cost-effectiveness (Diebold, 2003; Zhao et al., 2008).

Titanium is a metal, present in nature in various compounds, mostly oxides. The titanium dioxide has three different crystal structures: rutile, anatase and brookite (Winkler, 2003; Beeldens, 2006). Rutile is the most stable form of TiO_2 and because of that both anatase and brookite rearrange to rutile form at elevated temperature: 750 °C for brookite and 915 °C for anatase (Winkler, 2003). Pure brookite without rutile or anatase is rather difficult to prepare and therefore it is the less studied TiO_2 polymorph (Di Paola et al., 2008).

For the PCO application, anatase is superior to rutile because the conduction band location for anatase is more favourable for driving conjugate reactions involving electrons as well as very stable surface peroxide groups can be formed at the anatase during photo-oxidation reaction but not on the rutile surface (Ollis, 2000; Deng et al., 2002). The energy band-gaps of anatase and rutile are 3.20 and 3.02 eV, respectively (Fujishima et al., 1999).

The photogenerated holes are highly oxidizing. The redox potential for photogenerated holes is about 3.00 V (Palmisano and Sclafani, 1997). As a result of reaction with water, these holes can produce hydroxyl radicals (•OH) with slightly decreased redox potential of 2.80 V (Zhang et al., 1998 (a)). Both are more positive than that for ozone 2.07 V (Kaneko and Okura, 2002). The redox potential for conduction band electrons is –0.52 V allowing reducing dioxygen to superoxide, or to hydrogen peroxide. Depending upon the exact conditions, the holes, •OH radicals, O^{2-}, H_2O_2 and O_2 itself can all play important roles in the photocatalytic reaction mechanisms (Kaneko and Okura, 2002).

The basis of photocatalysis on TiO_2 is as follows (Reactions 1.1 – 1.6):

$$TiO_2 + h\nu \rightarrow TiO_2^* (e_{cb}^- + h_{vb}^+) \quad (1.1)$$

This is followed by formation of extremely reactive radicals, mostly •OH, at the semi-conductor surface and/or a direct oxidation of the polluting species (R):

$$h_{vb}^+ + H_2O \rightarrow \bullet OH + H^+ \quad (1.2)$$

$$h_{vb}^+ + OH^- \rightarrow \bullet OH_{ads} \quad (1.3)$$

$$h_{vb}^+ + R_{ads} \rightarrow R^+ \quad (1.4)$$

The ejected electrons react with electron acceptors such as oxygen adsorbed or dissolved in water:

$$e_{cb}^- + O_2 \rightarrow O_2^{\bullet -} \quad (1.5)$$

Also, the electrons and holes may recombine together in absence of electron donors or acceptors:

$$TiO_2^* (e_{cb}^- + h_{vb}^+) \rightarrow TiO_2 \quad (1.6)$$

Commercial pyrogenic titanium dioxide P25 (Evonik) formed in oxy-hydrogen flame is routinely used as a benchmark photocatalyst in oxidation of VOCs due to its unselective fairly good photoactivity towards wide spectra of pollutants, commercial availability and low cost.

However, since the PCO of many organic vapours on P25 is not sufficiently fast for commercial process implementation and the photocatalyst is often deactivated, more active catalysts should be developed.

Crystalline structure, catalyst surface area, pore size, density of OH-groups, surface acidity, number and nature of trap sites both in the lattice and at the surface, and adsorption-desorption characteristics play an important role in photocatalytic efficiencies (Sclafani and Herrmann, 1996). A large surface area can be the determining factor in certain photodegradation reactions, since a large amount of adsorbed organic molecules promotes the reaction rate (Bahnemann et al., 2002; Chen et al., 2004). However, powders with a large surface area are usually associated with large amounts of crystalline defects, which favour the recombination of electrons and holes leading to a poor photoactivity thus the balance between surface area and crystallinity is the most important to achieve the high photocatalytic activity (Carp et al., 2004).

Particle size of TiO_2 photocatalyst could be crucial for photocatalytic efficiency influencing the electron–hole recombination due to the migration time of photogenerated charge carriers proportional to the square of the particle size. Also, the overall number of surface active sites increases with decreasing particle size (Kortan et al., 1990). The increase of the PCO rate of pollutant with the decrease in the photocatalyst's primary particle sizes was studied by many researchers (Maira et al., 2000; Hao et al., 2002; Nam et al., 2004; Lin et al., 2006; Moiseev et al., 2011). Some authors suggest the existence of an optimum photocatalyst's particle size: Maira et al. (2000) reported the one of 7 nm for the PCO of trichloroethylene (TCE) in the gas-phase, Moiseev et al. (2011) –around 10 nm for the dichloroacetic acid (DCA) and 4-chlorophenol (4-CP) and Almquist and Biswas (2002) - in the range of 25 to 40 nm for PCO of phenol in aqueous solutions.

Jang et al. (2001) supported the idea that the decomposition of pollutant is affected by the photocatalyst's particle size: the increase in photocatalytically oxidised methylene blue was observed with the decrease in the particle sizes. However, they pointed also to the fact that the increase in anatase mass fraction has a more profound effect on the decomposition of pollutant than TiO_2 particle size. Deng et al. (2002) reported that the photocatalytic activities of titania pure anatase and pure rutile catalysts with comparable surface area and crystal size had a very close values in gas-phase oxidation of hexane. Reasons for higher photocatalytic activity of pyrogenic P25 with average particle size d_{TEM} of 21 nm and rutile fraction of 13 wt.%, as mentioned also in Paper III, were searched in the synergism of rutile and anatase fractions (Ohno et al., 2003; Komaguchi et al, 2006; Hurum et al., 2006). The theory of anatase and rutile synergism, however, was not supported by Datye (1995), Zhang et al. (1998 (b)), Jung and Grange (2001), Ohtani, et al. (2010) and Moiseev et al. (2011) concluding that the photocatalytic performance is governed by the characteristics of anatase particles; the high photoreactivity of P25 and other flame catalysts should be mainly attributed to the anatase phase.

1.2 Flame aerosol synthesis of titanium dioxide

Wet-chemical synthesis methods of nanopowders, for example incipient wetness impregnation, sol-gel, precipitation and grafting, include several post-treatment steps: filtration, washing, drying and calcination, whereas flame synthesis consists only of the evaporation of volatile metal precursors and their feeding to a flame. The metal precursor is converted into the metal oxide and starts forming particles by nucleation from the gas phase (Schwarz, 1995; Ertl et al., 1997).

Among various methods, the flame aerosol synthesis of nanopowders is favourable technique for controlling crystal structure, particle size and its distribution varying such process parameters as burner configuration, type of reactant and fuel. The aerosol flame technology is used in production of the commercial photocatalyst P25 (Evonik) (Strobel et al., 2006).

As has been previously shown, the flame aerosol synthesis allows synthesizing the catalysts with an optimum particle size for specific applications in catalytic processes (Ulrich, 1984; Pratsinis, 1998; Stark et al., 2002; Strobel et al., 2003; Strobel et al., 2006; Akurati et al., 2007). Nevertheless, the data on particle properties demonstrating higher photocatalytic activity is scarce due to the deficiency of well-defined series on particle sizes and phase compositions of photocatalysts.

The performance of flame aerosol synthesized photocatalysts exceeded, for example, commercial photocatalyst P25 and in some studies P90 in degradation of phenol, salicylic acid, DCA and 4-CP in aqueous solutions (Fotou et al., 1994; Fotou and Pratsinis, 1996; Moiseev et al., 2011). The data on the efficiency of flame synthesized TiO_2 catalysts in air treatment, however, are scarce, only the degradation of acetaldehyde and methanol in batch reactor was described by Balázs et al. (2011) using relatively coarse (over 50 nm) anatase nanoparticles from flame synthesis. Systematic studies on flame synthesized photocatalysts' series could correlate specific surface, size and structure properties with catalysts' photocatalytic activity.

1.3 Sulphation of titanium dioxide

The photocatalytic activity of TiO_2 depends on the lifetime of charge carriers generated on its surface. The surface recombination of electron–hole pairs in the absence of an electron donor or acceptor results in the deterioration of the quantum yield of the photocatalytic process. The inhibition of surface recombination of charge carriers can be provided by modifying the TiO_2 surface with anions, for example with sulphate (Kumar and Devi, 2011).

The sulphate ion forms S=O and O–S–O bonds in TiO_2, creating unbalanced charge on Ti-atoms, vacancies and defects in the titania structure (Jung and

Grange, 2001). In sulphated titanium dioxide, the O=S=O group anchored to the surface seems to trap electrons improving the oxidation process, retarding the recombination of holes and electrons induced by UV irradiation. The O=S=O species polarize the S=O bonds in presence of water to coordinate its molecules, giving an anchored sulphate, in which sulphur electron-deficient species are induced (Gómez et al., 2003). Also, the surface of more acidic TiO_2 samples remains free for interaction with the reagents due to the lower adsorption of PCO intermediates of acidic nature (Kozlov et al., 2003).

In gas-phase PCO Deng et al. (2002) showed higher conversions of hexane, benzene and methanol over sulphated TiO_2 and prolonged photocatalyst's stability compared to non-sulphated titania. The more stable performance of sulphated TiO_2 in PCO of toluene was not unequivocally explained in literature. Thus, Nakajima et al. (2005) and Keller et al. (2007) attributed the stable performance of sulphated TiO_2 in toluene PCO to a possibly increased electron–hole pairs formation and inhibited recombination of photogenerated charge carriers on photocatalyst's surface on the one hand and lower adsorption of toluene at the catalyst surface on the other hand. On the contrary, the higher adsorption of toluene on sulphated TiO_2 was reported by Muggli and Ding (2001). Also, acetone adsorption at low pollutant concentration was found to be improved together with the improved PCO performance due to the increased quantities of TiO_2 acidic sites and decreased quantities of basic sites on sulphated titania (Kozlov and Vorontsov, 2008).

1.4 Effect of humidity and temperature on the performance of gas-phase photocatalytic oxidation

The effect of relative humidity (RH) on photocatalytic degradation of gaseous VOCs has been a major research issue for several authors (Yamazaki et al., 2001; Lim and Kim, 2004; Demeestere et al., 2007; Korologos et al., 2011). However, there is still some debate about the role of water in photocatalytic degradation kinetics and catalyst lifetime. It appears that the effect of water vapour strongly depends on its concentration as well as on the type and concentration of the target VOC (Carp et al., 2004). In the absence of water vapour, the photocatalytic degradation of some chemical compounds, e.g., toluene, formaldehyde, is seriously retarded and the total mineralisation to CO_2 does not occur (Zhao and Yang, 2003). However, the excess water vapour on the catalyst surface will lead to the decreased reaction rate due to water molecules occupying the active sites on the catalyst surface (Zhao and Yang, 2003). Some explanations were proposed in terms of a dual effect of water vapour (Yamazaki et al., 2001; Krichevskaya and Preis, 2003; Lim and Kim, 2004): higher RH results in enhanced •OH radicals formation and suppressed electron–hole recombination, favouring the elimination rate of organic

compounds. On the other hand, the competition between the VOCs and water for the adsorption sites on the catalyst surface may reduce the adsorbed VOCs concentration, lowering the pollutants' elimination rate.

Temperature is one of the most important factors in gas–solid heterogeneous reactions affecting both adsorption–desorption and chemical conversion processes during photocatalytic degradation reactions. However, photocatalytic reactions are less sensitive to moderate variations in temperature because of the low thermal energy (kT = 0.026 eV at room temperature (Carp et al., 2004)) required for the activation of TiO_2. Since the activation energy is close to that of •OH radical formation, it is suggested that the degradation of pollutants is due to hydroxyl radical reactions (Fox and Dulay, 1993). The effect of temperature on the rate of oxidation could also be dominated by the rate of interfacial electron transfer to oxygen (Anpo et al., 1987).

At lower temperatures the desorption of PCO intermediates becomes the rate-limiting step of the process. The more rapid desorption from the catalyst at higher temperatures is probably an additional factor, leading to a larger effective surface area for the reaction. However, the adsorption of pollutant on the photocatalyst surface also decreases (Hermann, 1999; Carp et al., 2004).

Studies on the effect of temperature on PCO rate of VOCs showed that in a temperature range between 60 and 220 °C the photocatalytic TCE removal was not affected by temperature up to 125 °C, whereas removal efficiencies decreased significantly at higher temperatures (Avila et al., 1998; Sanchez et al., 1999). This was explained by limited TCE adsorption at elevated temperatures. Similar trends have been reported by Yamazaki et al. (2001): temperature showed no significant effect on tetrachloroethene elimination rate between 44 and 78 °C. Hager et al. (1999) noticed the decreased tri- and tetrachloroethene conversion with the temperature increased from 20 to 70 °C, giving the rate-limiting reactant adsorption as an explanation. On the contrary, Westrich et al. (2011) reported the range of temperatures, over which the PCO of ethylene was greater than 75%, laying between 60 and 350 °C with the maximum observed between 100 and 200 °C.

The effect of temperature on photocatalytic degradation of monocyclic aromatic VOC has been studied by Lichtin and Sadeghi (1998), Hager and Bauer (1999), and Belver et al. (2003). These authors reported no significant effect of temperature on benzene conversion in a range between 15 and 70 °C suggesting a minor number of adsorbed water molecules and hydroxyl radicals causing a decline of photocatalytic activity at higher temperatures. Wua et al. (2005), however, stated that at wider temperature scale benzene PCO rates increased with temperature below 160 to 180 °C, but decreased with further temperature growth above 160 to 180 °C. They also proposed that chemical reaction rate rise

with the increased temperature, although the pollutant adsorption on photocatalyst surface decreased with temperature.

The contradictions in the published results and the lack of knowledge on the impact of temperature, relative humidity and catalyst sulphation to the PCO performance in the abatement of target pollutants justify the experimental research undertaken into the PCO of chosen VOCs.

1.5 Objectives and strategies of the study

The objectives of the present research include:

- the estimation of the PCO potential in degradation of gaseous AN and its sensitivity towards reaction conditions,
- the identification of the products of AN PCO and thermal degradation,
- the establishing the potential of sulphated TiO_2 P25 catalyst improving the AN PCO performance,
- the evaluation of the gas-phase photocatalytic activity of the new flame synthesized F3 nanopowder photocatalyst compared to commercial P25 towards AN and toluene.

The stated objectives were achieved by experimental research undertaken into:

- the PCO of AN dependently on concentration of pollutant, air humidity and temperature, and the treated air residence time in a simple tubular reactor in continuous flow mode,
- the identification of AN volatile PCO products and products of AN temperature-programmed oxidation (TPO) obtained on the course of the transient and the continuous-flow studies,
- the PCO performance of sulphated TiO_2, P25 and the novel aerosol flame synthetic photocatalyst F3 was examined in full-factorial experiment varying the AN concentration, residence time and temperature; the performance of the F3 photocatalyst was also examined with toluene.

Deactivation of the photocatalysts and restoration of their activity was also studied.

2. MATERIALS AND METHODS

The equipment for the studies described in papers I, II and III varied as follows:

Paper I. The experimental runs were carried out in continuous-flow mode (Fig. 2.1) at the Department of Chemical Engineering of Tallinn University of Technology (TUT, Estonia) for the tests on the AN PCO process performance and effects of the process parameters and at the Department of Chemical Technology of Lappeenranta University of Technology (LUT, Finland) for the PCO products analysis. The equipment varied in analytical devices: Wilks MIRAN 1A infrared analyzer was used at TUT and Perkin Elmer 2000 FT-IR analyzer with Sirocco 10.6-m gas cell at LUT. Also, the reactors (Fig. 2.2 (a)) were sealed with silicone at TUT and PbO-glycerol cement at LUT. The air with dew point at 4 °C was used as the carrier gas at TUT, and synthetic air 80% N_2/20% O_2 was used at LUT as better suitable for analytical purposes.

Paper II. The experimental runs on AN PCO on sulphated P25 photocatalyst were performed in continuous-flow mode at TUT (Fig. 2.1). INTERSPEC 200-X FT-IR spectrometer with the Specac Tornado 8-m 1.33-l gas cell with ZnSe-windows was used as the gas analyzer; the reactor's (Fig. 2.2 (a)) sealant was changed to inorganic $ZnO\text{-}MnO_2\text{-}Na_2B_4O_7\text{-}Na_2O(SiO_2)_n$. The transient mode apparatus (Fig. 2.3) was used in studies of AN TPO and PCO by-products at the Department of Chemical and Biological Engineering of the University of Colorado at Boulder (CU-Boulder, USA).

Paper III. The experimental runs on AN and toluene PCO performance on F3 photocatalyst in comparison with P25 were carried out in continuous-flow mode at TUT. The INTERSPEC 200-X FT-IR was used for the gas analysis. The annular reactor was substituted with the lamp-in-pipe reactor shown in Fig. 2.2 (b). The F3 photocatalyst was synthesized at the Institute of Particle Technology and the Institute of Non-Metallic Materials at Clausthal University of Technology (TU Clausthal, Germany) and described in detail by Moiseev et al. (2011).

2.1 Continuous-flow mode

Gas-phase photocatalytic experimental equipment (Fig. 2.1) consists of a thermostatted reactor (Fig. 2.2), gas flow controllers, gas humidifier and infrared analyzer.

The temperature in the reactor was maintained within a range of 50 to 130 °C controlled by the heat of the lamp, reactor's insulation and heating tape with the temperature controller (Omega CN9000A).

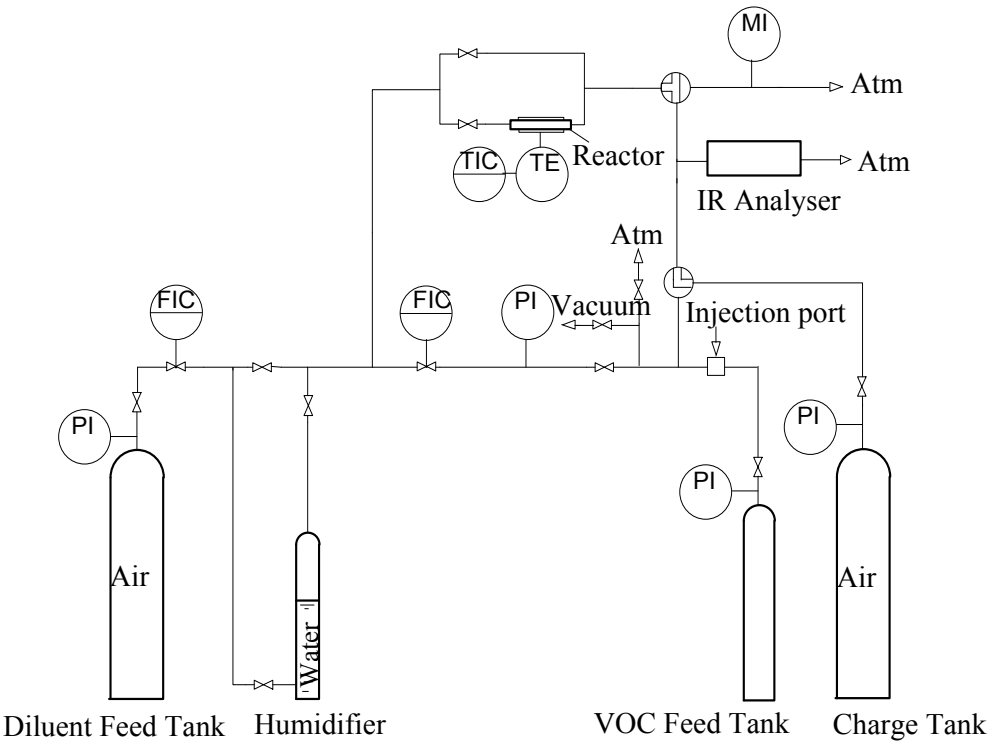

Fig. 2.1. Experimental device: PI – manometers, FIC – gas flow controllers, TE – thermo-pair, TIC – temperature controller, MI – gas humidity meter, Atm/Vacuum – connection to the atmosphere/vacuum

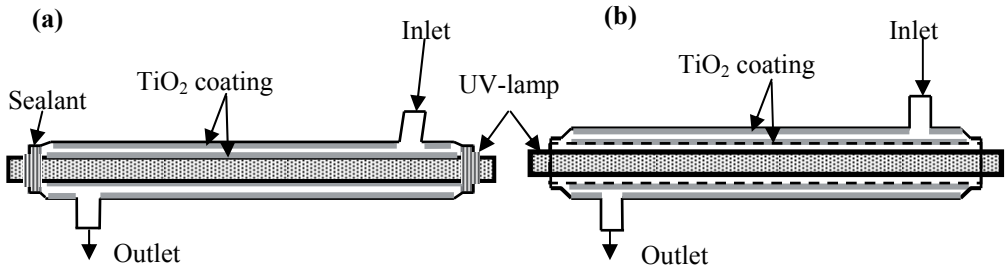

Fig. 2.2. Continuous flow-mode photocatalytic reactors: **(a)** – P25- and sulphated P25-coated reactor; **(b)** – lamp-in-pipe reactor.

The gas flow controllers provided gas flow rates from 0.5 to 4.0 L min^{-1} resulting in pollutant residence time in the reactor from 3 to 23 s. The in-line humidifier allowed the RH in the gas stream to be maintained from 0 to about 70% at 20 °C.

The VOC feed tank was charged with polluted air by tank evacuation and injection of a pollutant through the injection port. After 10-15 min of evaporation, the tank was pressurised with compressed air to 3 or 4 bar and left for the concentration balancing overnight. The diluent feed tank was used to dilute the polluted gas stream with the carrier gas – dry or humidified air.

The runs lasted for 60 min with the FT-IR outlet gas analysis after every 10 min.

At the end of each run, the photoreactor was treated by water vapour to restore photocatalyst activity for 2 h and then dried at 120 °C for 2 to 3 h (Paper I). In further studies (Paper II and III) at the end of each run, the photoreactor with UV lamp and air flow remained turned on was heated up to 180 °C for 3 h after the experiments with AN and for 15 h with toluene to restore the photocatalyst activity.

The annular lamp-in-pipe borosilicate glass reactor with total volume of 0.191 L composed of an inner glass tube (35 mm outer diameter) and an outer glass tube (45 mm inner diameter, 305 mm length) is shown in Fig. 2.2 (b).

A 365-nm 15 W low-pressure mercury luminescent UV-lamp (Philips) with UV-A intensity of 5 mW cm^{-2} at 365 nm was positioned coaxially in the reactor. The UV-A irradiance passing the TiO_2-coating to the reactor's annular clearance space was measured with the UVX Radiometer (Micropulse Technology) averaging 0.6 mW cm^{-2} for both P25- and sulphated P25-coated reactors, 0.46 for the F3 and 0.15 mW cm^{-2} for P25 in a lamp-in pipe reactor. No UV-A radiation was detected outside the reactor, i.e. no UV-A radiation passed through the double coating of titania.

2.2 Transient mode

The experimental device of transient study is schematically depicted in Figure 2.3 (a) and described in more detail by Larson and Falconer (1997). The reactor was surrounded by a UV-transparent furnace, and twelve 8 W ''black light'' UV-tubes (BLB Korea, type F8T5BLB), placed in a circle at a distance of 6 cm from the reactor for the reactor irradiation. The thermocouple provided feedback to a temperature controller, which produced a constant heating rate of 1 K s^{-1} during TPO. Radiometer measurements showed a UV intensity of 2.5 mW cm^{-2} and a maximum light intensity at 360 nm. The gas-phase species in the outlet stream were analysed by a quadrupole mass spectrometer (Balzers, QMA 125). Computer-controlled data acquisition simultaneously recorded

multiple mass signals, temperature, and elapsed time. A thin-film annular reactor was used for transient PCO. This photoreactor consists of two concentric Pyrex cylinders that form an annular region with a 1 mm gap (see Figure 2.3 (b)). The outer diameter of the inner cylinder is 20 mm, and the height - 160 mm.

PCO and TPO of AN were carried out in 20% O_2–80% He mixture flow (120 standard cm^3 min^{-1}). Before each experiment, the catalyst was heated to 400 °C in the O_2/He flow to obtain a reproducible oxide surface. The UV-lights were turned on and allowed to warm up for approximately 15 min before the cover over the reactor was removed to start the reaction.

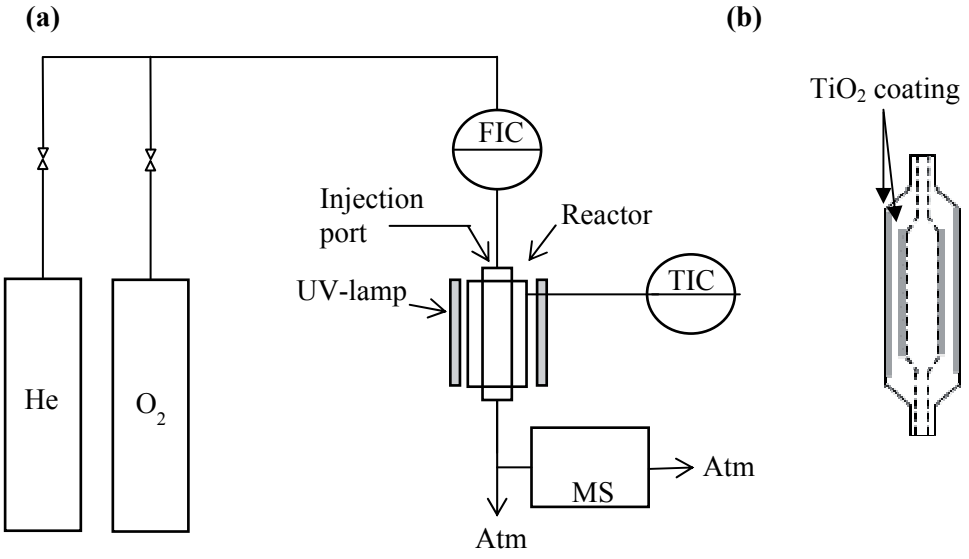

Figure 2.3. Experimental device outline **(a)**: FIC – gas flow controllers, TIC – temperature controller, MS – mass spectrometer, Atm – connection to the atmosphere; **(b)** - transient photocatalytic reactor.

2.3 Preparation of TiO_2 coatings

For photocatalytic experiments the photocatalyst material was fixed to the walls of the reactors.

The reactor's inner surface and the lamp were coated with TiO_2 and sulphated TiO_2 by about 50-times rinsing with 10-wt. % TiO_2 slurry in distilled water, each rinse followed by drying. The weighted TiO_2 coating mass corresponded to the catalyst loading of 1.4 or 2.0 mg TiO_2 per cm^2 of irradiated reactor surface (Paper I and II, respectively).

The total mass of the photocatalyst deposited in the reactor used in transient study made the TiO_2 coverage 1.9 mg cm^{-2} (Paper II).

In the lamp-in-pipe reactor the surface of the lamp was free from the catalyst that was fixed to the inner walls of the reactor. The weighted TiO_2 coating mass corresponded to the catalyst loading of 1.2 mg TiO_2 per cm^2 of irradiated reactor surface (Paper III).

The complete description of experimental conditions, materials and analysis could be found in the part "Experimental" in papers I – III. Experimental conditions are also summarised in Table 1.

Table 1. Consolidated table of experiments

Photo-catalyst	**AN inlet conc., ppmv**	**Toluene inlet conc., ppmv**	**Residence time, s**	**Relative humidity, %**	**Tempe-rature, °C**
P25	10; 25; 40; 100	-	3.2; 6.4; 12.8	0 and 66%	50; 130
Sulphated P25				0	
P25 transient study	20*; 40*; 100*	-	-	-	50; 90; 130
P25	10; 40; 100	10; 40; 100	3; 6; 11.5; 23	0	60; 130
F3					

* - the amounts of the AN injected were 0.1, 0.2 and 0.5 µl constituting the AN concentration of 20, 40 or 100 ppm referred to the volume of photocatalytic reactor.

3. RESULTS AND DISCUSSION

3.1 Products of acrylonitrile photocatalytic and thermal oxidation

Acrylonitrile readily reacted on the UV-irradiated TiO_2 catalyst to form carbon dioxide as the main gas-phase product. As shown in Fig. 1 (a) of Paper II, carbon dioxide formed immediately after the AN injection into the irradiated transient PCO reactor (about 60 s after the start of data acquisition). Carbon dioxide formation quickly dropped to zero when the UV lights were turned off.

To follow the desorption and thermal degradation of AN at corresponding temperatures, dark adsorption runs were carried out similarly to the PCO runs (Fig. 1 (b) of Paper II). No AN desorption or thermal degradation was observed at 50°C. At 90°C the thermal degradation was minor and slow. At 130 °C, however, the immediate desorption of AN along with its partial thermal degradation was followed: all three peaks of AN, HCN and CO_2 were detected instantly after the injection. Photocatalytic oxidation (Fig. 1 (a), Paper II) of injected AN resulted in no AN desorbed at any concentration or temperature within about 10 min of irradiation. No gaseous products other than carbon dioxide were observed in AN PCO at temperatures below 130 ºC. The HCN product was seen only at 130 ºC at the AN relative concentration as high as 100 ppm; the levels of HCN concentrations were much lower compared to dark adsorption. Relative concentrations of 20 and 40 ppm are not shown since no desorption of AN or its thermal degradation products, as well as no other gaseous PCO products besides CO_2, were detected at any temperature.

TPO study shows that PCO leads to practically total degradation of initial compound at lower AN concentrations (Fig. 2 (b), Paper II). The effectiveness of PCO found also a proof in the UV-TPO after PCO (not shown), where no desorbed AN was detected at any temperature and amounts adsorbed.

The study of the AN thermal oxidation products was carried out more thoroughly with the highest AN relative concentration of 100 ppm (Fig. 3, Paper II). The AN thermal degradation products mainly contain nitrogen at the same oxidation state as in the initial compound: only trace amounts of oxidised nitrogen were observed.

Fig. 1 of Paper I shows the infrared spectra of AN PCO gaseous products obtained at AN inlet concentration 40 ppmv, 130 °C, RH 0%, and residence time 6.4 s. The AN PCO volatile products, visible in infrared spectra, included nitrogen dioxide (in dry air), nitrous oxide, carbon dioxide, water, hydrogen cyanide and carbon monoxide. One could suppose a two-step mechanism involving initially the PCO of the CH_2=CH- moiety to CO_2 in adsorbed CH_2=CHCN. PCO of CN- moiety liberated by the first step of oxidation leads to

formation of nitrogen dioxide NO_2. The formation of nitrous oxide N_2O may be explained using the previously obtained knowledge.

The following reaction pathway for the PCO of nitrogen-containing compounds was proposed by Kolinko et al. (2007), Reaction 3.1:

$$HNO_{3(ads)} + NH_3 \rightarrow NH_4NO_{3(ads)} \text{ or}$$

$$\rightarrow N_2O + H_2O + HNO_3 + N_2 \quad (3.1)$$

Kolinko and Kozlov (2009) also showed that the N_2O formation occurs as a result of decomposition of hyponitrous acid (Reaction 3.2), which forms as a product of ammonia oxidation with OH-radical:

$$NH_3 + \bullet OH + O_2 \rightarrow HNO \rightarrow N_2O + H_2O \quad (3.2)$$

Also, formation of nitrous oxide N_2O, observed among the products, was described as a result of PCO of ammonia in the presence of nitrogen oxide NO (Perez-Ramirez et al., 2005).

The desorption of the original compound and its PCO products in TPO takes place simultaneously with their thermal degradation (Fig. 4, Paper II): the gaseous AN thermal degradation products, not all of which are shown at the TPO spectra, were CO_2, CO, H_2O, acetonitrile, HCN, NH_3, NO and NO_2. Nitrogen dioxide and water released starting at about 300 °C may be attributed to the thermal degradation of adsorbed nitric acid as the AN PCO by-product.

The emissions of hydrogen cyanide and nitrogen dioxide showed the opposite trends during AN TPO in transient mode. The degradation of cyanide took place during PCO of AN with lower amounts of HCN desorbed at higher temperatures and no HCN was observed during UV-assisted TPO at the lowest AN initial concentration and elevated temperature. On the contrary, ultimate AN PCO products, like nitrogen dioxide, carbon dioxide and water tended to accumulate during PCO and UV-assisted TPO. The detected CN moiety exhibits the behaviour expected for an intermediate species, leading to the final oxidation of the CN- moiety with increase in temperature or/and longer residence time.

3.2 Effect of process parameters on gas-phase photocatalytic oxidation of acrylonitrile

The PCO of AN was examined in a full-factorial experiments. The dependence of the conversion values of AN ($(C_{in} - C_{out})/C_{in}$ or $1 - C_{out}/C_{in}$, %) with different inlet concentrations on the residence time in reactor is shown in Fig. 2 of Paper I (run time 10 min) and 7 (b) of Paper II (run time 40 min).

The AN conversion degree increased with residence time, although not linearly. The complex mechanism of photocatalytic reactions including adsorption of the target compound followed by oxidation of adsorbed species, oxidation of by-products formed and desorption of by-products and unreacted initial compounds may explain the non-linear increase in AN conversion with residence time by, for example, the slowdown in desorption processes and therefore retardation of adsorption of AN.

The poisoning of the photocatalyst was observed during PCO of AN at higher inlet concentrations and residence time of less than 12.8 s at 130 °C (Paper I). This indicates that some species adsorbed on the photocatalyst surface during PCO of AN and caused the deactivation. Thus, the rate-limiting stage for AN complete oxidation is the PCO of the adsorbed oxidation intermediates. The degradation rates of the intermediates seem to be slower than the degradation rate of AN. During PCO of AN at all inlet concentrations up to 100 ppmv and residence time of more than 12.8 s at 130 °C no poisoning of the photocatalyst was observed for 1 h of continuous run, the degradation percent of AN remained the same during this time showing no catalyst deactivation. Because intermediates form on the surface and their appearance depends on their rates of formation, desorption, oxidation rate and displacement by other species, the reactions are neither first-order nor diffusion-controlled. This indicated that the rate of the process limited by a surface reaction with an order greater than one would be dependent on the AN concentration.

Fig. 3 (a) of Paper I shows that the presence of humidity (RH 66%) at 130 °C do not cause alterations in the degradation rate of the AN in 10 min from the start of the experiments at small inlet concentrations of AN (10 and 40 ppmv). A slight decrease in AN conversion was observed at high (100 ppmv) AN concentration in presence of water vapour. The decrease in the PCO rate in the presence of humidity may be explained by the competitive adsorption of water and VOC molecules on the photocatalyst surface.

After 1 h of continuous run (Fig. 3 (b) of Paper I), the dual effect of water vapour was observed. At small inlet concentrations of AN the decrease in degradation from 10 to 20% compared to dry air was observed. On the contrary, the degradation of AN with an initial concentration of 100 ppmv in 1 h was higher in humid air: the conversion of AN in dry air dropped approximately for 19%, while in humid it decreased only for 4%, thus showing the favourable effect of water vapour extending the photocatalyst deactivation time at higher AN concentrations. The durability factor (Einaga et al, 2002) defined here as the ratio of the AN degradation fractions at 1 h to those at the first 10 minutes, increased from 0.32 to 0.83 with an increase in relative air humidity at AN inlet concentration of 100 ppmv.

An important role of water vapour in the regeneration of the photocatalyst was observed: entire restoration of the photocatalyst activity was achieved by 2-h PCO of adsorbed oxidation by-products in humid airflow, the colour of the photocatalyst turned from yellowish to white. UV-irradiation of the photocatalyst layer in dry air did not restore the photocatalyst's activity; even the colour of the photocatalyst remained yellow.

The minor negative effect of increasing temperature from 60 to 130 °C was observed during PCO of AN and toluene (Papers I and III) over plain TiO_2. PCO reactions are often insensitive towards temperature changes as adsorption is deteriorated and oxidation reactions are usually accelerated with the temperature growth. However, a noticeable effect of temperature on the PCO of AN was observed in the character and quantities of the AN PCO products. Higher temperature resulted in deeper oxidation of AN on P25 showing more profound oxidation of hydrogen cyanide and therefore the higher yield of nitrogen dioxide (Fig. 4, Paper I).

The temperature increase, however, had positive effect on the performance of sulphated P25 photocatalyst and on the character of gaseous products emissions during PCO of AN on F3 (see Section 3.2.2 The impact of temperature and residence time on PCO Performance, Paper II, and Section 3.2 PCO of acrylonitrile, Paper III).

3.3 Photocatalytic oxidation of acrylonitrile over sulphated P25 photocatalyst

The infrared spectra of AN PCO gaseous products formed during the oxidation on sulphate TiO_2 differ from the ones on P25 in part of HNCO, appearance of which was not observed during AN PCO on P25. Isocyanic acid formed as a result of oxygen addition to HCN hydrolyses further to ammonia and CO_2. Another difference consists of the absence of NO_2 clearly seen at AN PCO on plain P25. The acidic surface of sulphated titania thus presume to induce the formation and adsorption of nitric acid and ammonia ions (see Paper II, section 3.2.1. PCO by-products).

The drastic negative effect of temperature decreasing from 130 to 60 °C on AN PCO conversion was observed on sulphated P25 (Fig. 8, Paper II). The 'reaction rate-adsorption' balance at sulphated P25 appears to be dramatically negatively influenced by the temperature decrease practically zeroing its performance. This behaviour is sometimes attributed to thermal catalytic reactions. This possibility is supported by the observation of the minor thermal decomposition reaction at 130 °C and the absence of any reaction at 60 °C.

Although thermal catalytic reactions are thought to be similar on both P25 and sulphated P25, however, they poison P25 more rapidly since P25 better

adsorption properties and faster PCO reactions along with AN thermal degradation produce more by-products accumulating on photocatalyst surface.

The dependence of AN PCO conversion rate on its initial concentration at retention time increased from 6.3 to 12.8 s on sulphated TiO_2 has a spasmodic character (Fig. 7 (b), Paper II). It could be explained by the changes in the reaction pathway and kinetics. The formation of HNCO at retention time of 12.8 s could start to prevail oxidising to CO_2 and ammonia, possibly further transforming to N_2O and easily desorbing. Thus the accumulation of the reaction intermediates on the sulphated TiO_2 surface could catalyse the conversion at longest retention times.

Thus, sulphated P25 showed better photocatalytic activity at longer retention times and higher temperatures. The AN PCO performance on sulphated P25 was strongly deteriorated at low temperature and shorter retention times.

3.4 Photocatalytic oxidation of acrylonitrile and toluene over flame synthesized F3 photocatalyst

The superior character of flame aerosol synthesized catalyst over the benchmark P25 was confirmed for the gas-phase PCO similar to the previously observed in aqueous reactions: both well-adsorbed aliphatic DCA (aqueous) and AN (gas), and weakly adsorbed 4-CP (aqueous) and toluene (gas) yielded better to PCO at the flame aerosol catalyst (Moiseev et al., 2011; Paper III).

The primary particle size, higher anatase content and lower agglomeration degree present the apparent reasons of improved PCO performance for AN adsorbable at the catalyst's surface. The improved performance in poorly adsorbable toluene oxidation, however, cannot be solely explained by larger adsorbing surface: non-adsorbable VOCs should mostly be oxidized by surface OH-radicals, the yield of which also, but not exclusively, is dependent on the water content at the catalyst surface. The water surface content showed disproportional relation to the photocatalysts' specific surface or saturation time – two-fold increased contact surface of F3 adsorbed three-fold amount of water compared to P25 (see Fig. 3, Paper III), which may also explain accelerated toluene PCO with F3 at all temperatures studied.

On the other hand the enhanced dehydration of F3 surface at elevated temperature causes a poorer catalyst's performance in PCO of hydrogen cyanide during PCO of AN. The more incomplete HCN oxidation at elevated temperature with F3 compared to P25 may follow two explanation patterns, the dehydration of the catalyst surface resulted in reduced OH-radicals production at higher temperature (130 ºC), and the HCN volatility drastically surpassing the volatility of AN.

At 60 °C equal amounts of HCN appear at the same time with both photocatalysts, thus making the overall yield of gaseous hydrogen cyanide per unit of oxidised AN higher for P25, where degradation of AN is incomplete (Fig. 5, Paper III, see section 3.2 PCO of acrylonitrile).

The faster restoration of F3 photocatalytic activity and slower photocatalyst's deactivation could be explained by better UV-light transparency of F3 coating along with its enhanced oxidative ability.

CONCLUSIONS

The increased amount of personnel time spent in indoor environment makes the science confront the VOCs as the most abundant chemical pollutants in the indoor air. Photocatalytic oxidation of indoor VOCs over titanium dioxide could be efficient pollutant degradable abatement technology. In present study the author used toluene characterizing the performance of novel catalyst compared to the commercially available one thus creating a new knowledge in effective and reliable method of problematic air pollutant abatement. The author failed to find published information on gas-phase PCO of AN, thus obtaining the new knowledge on the PCO chemistry.

The objectives of the present research included the study of the pathway of AN PCO and estimation of the gas-phase PCO performance of new flame synthesized photocatalyst F3 and sulphated P25 in comparison with commercial P25 titanium dioxide. The observed features of the photocatalysts found explanation.

Acrylonitrile readily undergoes photocatalytic degradation in gas-solid systems by using titanium dioxide. The main reaction products were carbon dioxide, water and nitrogen dioxide or adsorbed nitric acid; the intermediate products hydrogen cyanide, nitrous oxide and carbon monoxide were observed. The thermal oxidation with and without simultaneous UV-irradiation allowed following the CN^- group transformation to nitrogen oxides: HCN behaved as an intermediate by-product degrading along with the PCO, which resulted in the accumulation of nitrogen dioxide. The PCO at temperatures about 90 °C and higher allowed complete degrading of intermediate hydrogen cyanide at initial relative concentrations of AN up to 40 ppm.

The presence of water vapour extended the photocatalyst deactivation time at higher AN concentrations. An important role of water vapour in the regeneration of the photocatalyst was also observed: entire restoration of the photocatalyst activity was achieved by PCO of adsorbed oxidation by-products in humid airflow.

The effect of temperature increasing from 60 to 130 ºC was observed to be slightly negative in terms of AN degradation. However, the effect of increased temperature was noticeable in terms of the character and yields of the PCO products on P25: HCN content diminished with growing content of NO_2 at elevated temperature.

Sulphated P25 showed better photocatalytic activity at longer retention times and higher temperatures. The AN PCO performance on sulphated P25 was strongly deteriorated at low temperature and shorter retention times.

The superior character of the flame aerosol synthesized catalyst over the commercial P25 titanium dioxide in gas-phase PCO was established for degradation of aliphatic heteroatomic acrylonitrile and aromatic toluene. This demonstrates the unselective character of newly designed catalyst universal for both gaseous and aqueous PCO reactions. The new catalyst surpasses the commercial P25 in, for example, toluene oxidation for over 50 % under similar experimental conditions. Slower deactivation and faster complete restoration of catalytic activity of flame synthesized catalyst under UV-A-radiation are also the new catalyst's beneficial key features.

The intense dehydration of the reduced size anatase crystallites in the new catalyst results in decreased OH-radicals production at elevated temperature. Along with the enhanced desorption, this causes a poorer catalyst's performance in PCO of HCN, the PCO product of acrylonitrile. The process safety thus requires lower operational temperatures.

The right of photocatalysis technology for air remediation to existence in future will be depending to a great extent on the development of effective catalytic materials possessing unselective activity towards VOCs.

REFERENCES

1. Akurati, K. K., Vital, A., Fortunato, G., Hany, R., Nueesch, F., Graule, T. 2007. Flame synthesis of TiO_2 nanoparticles with high photocatalytic activity. - Solid State Sciences, 9, p. 247–257.
2. Almquist, C. B., Biswas, P. 2002. Role of synthesis method and particle size of nanostructured TiO_2 on its photoactivity. - Journal of Catalysis, 212, p. 145–156.
3. Anpo, M., Shima, T., Kodama, S., Kubokawa, Y. 1987. Photocatalytic hydrogenation of propyne with water on small-particle titania: size quantization effects and reaction intermediates. - Journal of Physical Chemistry B, 91, p. 4305–4310.
4. ATSDR - Agency for Toxic Substances and Disease Registry, Toxicological Profile for Toluene, U.S. Public Health Service, U.S. Department of Health and Human Services. Atlanta: 1994.
5. Augugliaro, V., Coluccia, S., Loddo, V., Marchese, L., Martra, G., Palmisano, L., Schiavello, M. 1999. Photocatalytic oxidation of gaseous toluene on anatase TiO_2 catalyst: mechanistic aspects and FT-IR investigation. - Applied Catalysis B: Environmental, 20, p. 15–27.
6. Avila P., Bahamonde A., Blanco J., S´anchez B., Cardona A. I., Romero M. 1998. Gas-phase photo-assisted mineralization of volatile organic compounds by monolythic titania catalysts. - Applied Catalysis B: Environmental, 17, p. 75–88.
7. Bahnemann, D. W., Kholuiskaya, S. N., Dillert, R., Kulak, A. I., Kokorin, A. I. 2002. Photodestruction of dichloroacetic acid catalyzed ny nano-sized TiO_2 particles. - Applied Catalysis B: Environmental, 36, p. 161-169.
8. Balázs, N., Gácsi, A., Pallagi, A., Mogyorósi, K., Alapi, T., Sipos, P., Dombi, A. 2011. Comparison of the liquid and gas phase photocatalytic activity of flame-synthesized TiO_2 catalysts: the role of surface quality. - Reaction Kinetics, Mechanisms, and Catalysis, 102, p. 283–294.
9. Beeldens, A. An environmental friendly solution for air purification and self-cleaning effect: the application of TiO_2 as photocatalyst in concrete. - http://www.crr.be/pdf/tra_beeldens_txt.pdf (03.2008).
10. Belver, C., Lopez-Munoz, M. J., Coronado, J. M., Soria, J. 2003. Palladium enhanced resistance to deactivation of titanium dioxide during the photocatalytic oxidation of toluene vapors. - Applied Catalysis B: Environmental, 46, p. 497–509.
11. Byrd, G., Fowler, K., Hicks, R., Lovette, M., Borgerdin, M. 1990. Isotope dilution gas chromatography-mass spectrometry in the determination of benzene, toluene, styrene and acrylonitrile in mainstream cigarette smoke. - Journal of Chromatography A, 503, p. 359–436.

12. Carp, O., Huisman, C. L., Reller, A. 2004. Photoindused reactivity of titanium dioxide. – Progress in Solid State Chemistry, 32, p. 33 - 177.
13. Chen, J., Kou, S. C., Poon, C. S. 2011. Photocatalytic cement-based materials: Comparison of nitrogen oxides and toluene removal potentials and evaluation of self-cleaning performance. – Building and Environment, 46, p. 1827-1833.
14. Chen, Y., Wang, K., Lou, L. P. 2004. Photodegradation of dye pollutants on silica gel supported TiO2 particles under visible light irradiation, - L.,Journal of Photochemistry and Photobiology A: Chemistry, 163, p. 281-287.
15. Datye, A. K., Riegel, G., Bolton J. R., Huang, M., Prairie, M. R. 1995. Microstructural Characterization of a Fumed Titanium Dioxide Photocatalyst. - Journal of Solid State Chemistry, 115, p. 236-239.
16. Demeestere K., Dewulf J., Van Langenhove H. 2007. Heterogeneous photocatalysis as an advanced oxidation process for the abatement of chlorinated, monocyclic aromatic and sulphurous volatile organic compounds in air: state of the art. - Critical Reviews in Environmental Science and Technology, 37, p. 489 - 538.
17. Deng, X. Y., Yue, Y. H., Gao, Z. 2002. Gas-phase photo-oxidation of organic compounds over nanosized TiO_2 photocatalysts by various preparations. - Applied Catalysis B: Environmental, 39, p. 135-147.
18. Di Paola, A., Cufalo, G., Addamo, M., Bellardita, M., Campostrini, R., Ischia, M., Ceccato, R., Palmisano, L. 2008. Photocatalytic activity of nanocrystalline TiO_2 (brookite, rutile and brookite-based) powders prepared by thermohydrolysis of $TiCl_4$ in aqueous chloride solutions. - Colloids and Surfaces A: Physicochemical and Engineering Aspects, 317, p. 366-376.
19. Dibble, L. A., Raupp, G. B. 1990. Kinetics of the gas-solid heterogeneous photocatalytic oxidation of trichloroethylene by near UV illuminated titanium-dioxide. - Catalysis Letters, 4, p. 345-354.
20. Diebold, U. 2003. The surface science of titanium dioxide. - Surface Science Reports, 48, p. 53-229.
21. Einaga, H., Futamura, S., Ibusuki, T. 2002. Heterogeneous photocatalytic oxidation of benzene, toluene, cyclohexene and cyclohexane in humidified air: comparison of decomposition behaviour on photoirradiated TiO_2 catalyst. - Applied Catalysis B: Environmental, 38, p. 215–225.
22. EPA - Environmental Protection Agency, Integrated Risk Information System (IRIS) on Toluene, National Center for Environmental Assessment, Office of Research and Development. Washington: 1999.
23. Ertl, G., Knözinger, H., Weitkamp, J. 1997. Handbook of Heterogeneous Catalysis. Wiley-VCH, Weinheim.

24. Foster, H. A., Ditta, I. B., Varghese, S., Steele, A. 2011 Photocatalytic disinfection using titanium dioxide: spectrum and mechanism of antimicrobial activity. - Applied Microbiology and Biotechnology, 90, p. 1847-1868.
25. Fotou, G. P., Pratsinis, S. E. 1996. Photocatalytic destruction of phenol and salicylic acid with aerosol-made and commercial titania powders. - Chemical Engineering Communications, 151, p. 251–269.
26. Fotou, G. P., Vemury, S., Pratsinis, S. E. 1994. Synthesis and evaluation of titania powders for photodestruction of phenol - Chemical Engineering Science, 49, p. 4939–4948.
27. Fox, M. A., Dulay, M. T. 1993. Heterogeneous photocatalysis. - Chemical Reviews, 93, p. 341–357.
28. Fujishima, A., Hashimoto, K., Watanabe, T. 1999. TiO_2 photocatalysis. Fundaments and applications, 1st edition. Tokyo: BKC.
29. Fujishima, A., Honda, K. 1972. Electrochemical Photolysis of Water at a Semiconductor Electrode. – Nature, 238, p.37-38
30. Fujishima, A., Zhang, X., Tryk, D. A. 2008. TiO_2 photocatalysis and related surface phenomena. - Surface Science Reports, 63, p. 515–582.
31. Gamage, J., Zhang, Z. 2011. Applications of Photocatalytic Disinfection. - International Journal of Photoenergy 2010, 1-11.
32. Gervasini, A., Ragaini, V. 2000. Catalytic technology assisted with ionization/ozonization phase for the abatement of volatile organic compounds. - Catalysis Today, 60, p. 129-138.
33. Gómez, R., Lópeza, T., Ortiz-Islasa, E., Navarreteb, J., Sánchezc, E., Tzompanztzic, F., Bokhimid, X. 2003. Effect of sulfation on the photoactivity of TiO_2 sol–gel derived catalysts. - Journal of Molecular Catalysis A: Chemical, 193, p. 217-226.
34. Hager S., Bauer R. 1999. Heterogeneous photocatalytic oxidation of organics for air purification by near UV irradiated titanium dioxide. - Chemosphere, 38, p. 1549–1559.
35. Hager, S., Bauer, R., Kudielka, G. 1999. Photocatalytic oxidation of gaseous chlorinated organics over titanium dioxide. – Chemosphere, 8, p. 1219 – 1225.
36. Hao, W. C., Zheng, S. K., Wang C., Wang, T. M. 2002. Comparison of the photocatalytic activity of TiO_2 powder with different particle size. - Journal of Materials Science Letters, 21, p. 1627-1629.
37. Hoffmann, M. R., Moss, J. A., Baum, M. M. 2011. Artificial photosynthesis: semiconductor photocatalytic fixation of CO_2 to afford higher organic compounds. - Dalton Transactions, 40, p. 5151-5158.
38. Hung, W. C., Chu, H. 2006. Catalytic incineration of acrylonitrile with platinum supported on Al_2O_3. - Journal of Environmental Engineering, 132, p. 1482-1488.

39. Hurum, D. C., Agrios, A. G., Crist, S. E., Gray, K. A., Rajh, T., Thurnauer, M. C. 2006. Probing reaction mechanisms in mixed phase TiO_2 by EPR. - Journal of Electron Spectroscopy and Related Phenomena, 150, p. 155–163.
40. Jang, H. D., Kim, S.-K., Kim, S.-J. 2001. Effect of particle size and phase composition of titanium dioxide nanoparticles on the photocatalytic activity. - Journal of Nanoparticle Research, 3, p. 141–147.
41. Jung, S., Grange, P. 2001. Evidence of Correlation between Electronic Density and Surface Acidity of Sulfated TiO_2. - Catalysis Letters, 76, p. 27 – 30.
42. Kaneko, M., Okura, I. 2002. Photocatalysis. Science and technologies. Tokyo: Kodansha Ltd.
43. Keller, N., Barraud, E., Bosc, F., Edwards, D., Keller, V. 2007. On the modification of photocatalysts for improving visible light and UV degradation of gas-phase toluene over TiO_2. - Applied Catalysis B: Environmental, 70, p. 423–430.
44. Kolinko, P. A., Kozlov, D. V. 2009. Products distribution during the gas phase photocatalytic oxidation of ammonia over the various titania based photocatalysts. - Applied Catalysis B: Environmental, 90, p. 126 – 131.
45. Kolinko, P. A., Kozlov, D. V., Vorontsov, A. V., Preis, S. V. 2007. Photocatalytic oxidation of 1,1-dimethyl hydrazine vapours on TiO_2: FTIR in situ studies. - Catalysis Today, 122, p. 178 – 185.
46. Komaguchi, K., Nakano, H., Araki, A., Harima, Y. 2006. Photoinduced electron transfer from anatase to rutile in partially reduced TiO_2 (P-25) nanoparticles: An ESR study. - Chemical Physics Letters, 428, p. 338–342.
47. Korologos, C. A., Philippopoulos, C. J., Poulopoulos, S. G. 2011. The effect of water presence on the photocatalytic oxidation of benzene, toluene, ethylbenzene and m-xylene in the gas-phase. - Atmospheric Environment, 45, p. 7089-7095.
48. Kortan, A. R., Hull, R., Opila, R. L., Bawendi, M. G., Steigerwald, M. L., Carroll, P. J., Brus, L. E. 1990. Nucleation and growth of cadmium selendie on zinc sulfide quantum crystallite seeds, and vice versa, in inverse micelle media. – Journal of American Chemical Society, 112, p. 1327 – 1332.
49. Kozlov, D. V., Vorontsov, A.V. 2008. Sulphuric acid and Pt treatment of the photocatalytically active titanium dioxide. - Journal of Catalysis, 258, p. 87-94.
50. Kozlov, D., Bavykin, D., Savinov, E. 2003. Effect of the acidity of TiO_2 surface on its photocatalytic activity in acetone gas-phase oxidation. - Catalysis Letters, 86, p. 169-172.
51. Kozlova, E. A., Safatov, A. S., Kiselev, S. A., Marchenko, V. Y., Sergeev, A. A., Skarnovich, M. O., Emelyanova, E. K., Smetannikova,

M. A., Buryak, G. A., Vorontsov, A. V. 2010. Inactivation and Mineralization of Aerosol Deposited Model Pathogenic Microorganisms over TiO_2 and Pt/TiO_2, - Environmental Science & Technology, 44, p. 5121-5126.

52. Krichevskaya, M., Preis, S. 2003. Gas-phase photocatalytic oxidation of styrene in a simple tubular TiO_2 reactor. - Journal of Advanced Oxidation Technologies, 6, p. 150 - 157.
53. Kumar, S. G., Devi, L. G. 2011. Review on Modified TiO2 Photocatalysis under UV/Visible Light: Selected Results and Related Mechanisms on Interfacial Charge Carrier Transfer Dynamics. - Journal of Physical Chemistry A, 115, p. 13211–13241.
54. Léonard, A., Gerber, G. B., Stecca, C., Rueff, J., Borba, H., Farmer, P. B., Sram, R. J., Czeizel, A. J., Kalina, I. 1999. Mutagenicity, carcinogenicity, and teratogenicity of acrylonitrile. - Mutation Research, 436, p. 263–283.
55. Lichtin, N. N., Sadeghi, M. 1998. Oxidative photocatalytic degradation of benzene vapor over TiO_2. - Journal of Photochemistry and Photobiology: A Chemistry, 113, p. 81–88.
56. Lim, T. H., Kim, S. D. 2004. Trichloroethylene degradation by photocatalysis in annular flow and annulus fluidized bed photoreactors. - Chemosphere, 54, p. 305–312.
57. Lin, H., Huang, C. P., Li, W., Ni, C., Ismat Shah, S., Tseng, Y-H. 2006. Size dependency of nanocrystalline TiO_2 on its optical property and photocatalytic reactivity exemplified by 2-chlorophenol. - Applied Catalysis B: Environmental, 68, p. 1–11.
58. Lin, Y. 2008. Photocatalytic activity of TiO_2 nanowire arrays. - Materials Letters, 62, p. 1246–1248.
59. Maira, A. J., Yeung, K. L., Lee, C. Y., Yue, P. L., Chan, C. K. 2000. Size effects in gas-phase photo-oxidation of trichloroethylene using nanometer-sized TiO2 catalysts. - Journal of Catalysis, 192, p. 185–196.
60. Méndez-Román, R., Cardona-Martínez, N. 1998. Relationship between the formation of surface species and catalyst deactivation during the gas phase photocatalytic oxidation of toluene. - Catalysis Today, 40, p. 353–365.
61. Mo, J., Zhang, Y., Xu, Q., Joaquin Lamson, J., Zhao, R. 2009. Photocatalytic purification of volatile organic compounds in indoor air: A literature review. - Atmospheric Environment, 43, p. 2229–2246.
62. Moiseev, A., Qi, F., Deubener J., Weber A. 2011. Photocatalytic activity of nanostructured titanium dioxide from diffusion flame synthesis. - Chemical Engineering Journal, in press.
63. Muggli, D. S., Ding, L. 2001. Photocatalytic performance of sulfated TiO_2 and Degussa P-25 TiO_2 during oxidation of organics. - Applied Catalysis B: Environmental, 32, p. 181-194.

64. Nakajima, A., Obata, H., Kameshima, Y., Okada K. 2005. Photocatalytic destruction of gaseous toluene by sulfated TiO_2 powder. - Catalysis Communications, 6, p. 716-720.
65. Nam, H.-J., Amemiya, T., Murabayashi, M., Itoh, K. 2004. Photocatalytic activity of sol-gel TiO_2 thin films on various kinds of glass substrates: The effects of Na^+ and primary particle size. - The Journal of Physical Chemistry B, 108, p. 8254-8259.
66. Obee, T. N., Brown, R. T. 1995. TiO_2 photocatalysis for indoor air applications – effects oh humidity and trace contaminant levels on the oxidation rates of formaldehyde, toluene, and 1,3-butadiene. - Environmental Scence &. Technology, 29, p. 1223-1231.
67. Ohno, T., Tokieda, K., Higashida, S., Matsumura, M. 2003. Synergism between rutile and anatase TiO_2 particles in photocatalytic oxidation of naphthalene. - Applied Catalysis A: General, 244, p. 383–391.
68. Ohtani, B., Prieto-Mahaney, O. O., Li, D., Abe, R. 2010. What is Degussa (Evonik) P25? Crystalline composition analysis, reconstruction from isolated pure particles and photocatalytic activity test. - Journal of Photochemistry and Photobiology A: Chemistry, 216, p. 179-182.
69. Ollis, D. F. 2000. Photocatalytic purification and remediation of contaminated air and water. - Comptes Rendus de l'Académie des Sciences - Series IIC: Chemistry, 3, 405–411.
70. Palmisano, L., Sclafani, A. 1997. Thermodynamics and kinetics for heterogeneous photocatalytic processes. In: Schiavello, M. (ed.), Heterogeneous photocatalysis. Chichester: Wiley & Sons, p.109–132.
71. Paz, Y. 2010. Application of TiO_2 photocatalysis for air treatment: Patents' overview. - Applied Catalysis B: Environmental, 99, p. 448-460.
72. Perez-Ramirez, J., Kondratenko, E., Kondratenko, V., Baerns, M. 2005. Selectivity-directing factors of ammonia oxidation over PGM gauzes in the Temporal Analysis of Products reactor: Secondary interactions of NH3 and NO. - Journal of Catalysis, 229, p. 303-313.
73. Piera, E., Ayllon, J. A., Domenech, X., Peral, J. 2002. TiO_2 deactivation during gas-phase photocatalytic oxidation of ethanol. - Catalysis Today, 76, p. 259–270.
74. Pratsinis, S. E. 1998. Flame aerosol synthesis of ceramic powders, - Progress in Energy and Combustion Science, 24, p. 197-219.
75. Sanchez B., Cardona A. I., Romero M., Avila P., Bahamonde A. 1999. Influence of temperature on gas-phase photo-assisted mineralization of TCE using tubular and monolithic catalysts. - Catalysis Today, 54, p. 369–377.
76. Scherer, G., Engl, J., Urban, M., Gilch, G., Janket, D., Riedel, K. 2007. Relationship between machine-derived smoke yields and biomarkers in cigarette smokers in Germany. - Regulatory Toxicology and Pharmacology, 47, p. 171–183.

77. Schwarz, J. A. 1995. Methods for preparation of catalytic materials. - Chemical Reviews, 95, p. 477–510.
78. Sclafani, A., Herrmann, J. M. 1996. Comparison of the Photoelectronic and Photocatalytic Activities of Various Anatase and Rutile Forms of Titania in Pure Liquid Organic Phases and in Aqueous Solutions. - Journal of Physical Chemistry, 100 (32), p. 13655–13661.
79. Shiraishi, Y., Hirai, T. 2008. Selective organic transformations on titanium oxide-based photocatalysts. - Journal of Photochemistry and Photobiology C – Photochemistry Reviews, 9, p. 157-170.
80. Shivaraju, H. P. 2011. Removal of Organic Pollutants in the Municipal Sewage Water by TiO_2 based Heterogeneous Photocatalysis. - International Journal of Environmental Science, 1, p. 911-923.
81. Siham, O., Hussein, K. 2009. Synthesis of benzaldehyde from toluene by a photocatalytic oxidation using TiO_2-pillared clays. - Journal of Photochemistry and Photobiology A-Chemistry, 207, p. 268-273.
82. Stark, W. J., Pratsinis, S. E. 2002. Aerosol flame reactors for manufacture of nanoparticles. - Powder Technology, 126, p. 103-108.
83. Strobel, R., Baiker, A., Pratsinis, S. 2006. Aerosol flame synthesis of catalysts. - Advanced Powder Technology, 17, p. 457–480.
84. Strobel, R., Stark, W. J., Mädler, L., Pratsinis, S. E., Baiker, A. 2003. Flame-made platinum/alumina: structural properties and catalytic behaviour in enantioselective hydrogenation. - Journal of Catalysis, 213, p. 296-304.
85. Ulrich, G. D. 1984. Flame synthesis of fine particles, C&EN 6, 22-29.
86. Van der Vaart, D. R., Vatvuk, W. M., Wehe, A. H. 1991. Thermal and catalytic incinerators for the control of VOCs - Journal of the Air & Waste Management Association, 41(1), p. 92- 98.
87. Wang, S., Ang, H. M., Tade, M. O. 2007. Volatile organic compounds in indoor environment and photocatalytic oxidation: State of the art. - Environment International, 33, p. 694–705.
88. Westrich, T. A., Dahlberg, K. A., Kaviany, M., Schwank, J. 2011. High-Temperature Photocatalytic Oxidation of Ethylene on TiO_2. - Journal of Physical Chemistry C, 115, p. 16537-16543.
89. WHO. 2010. WHO guidelines for indoor air quality: selected pollutants. World Health Organization 2010, ISBN 978 92 890 0213 4, pp. 454
90. Winkler, J. 2003. Titanium Dioxide. Hannover: Vinsentz Network.
91. Wua, J.-F., Hung, C.-H., Yuan, C.-S. 2005. Kinetic modeling of promotion and inhibition of temperature on photocatalytic degradation of benzene vapour. - Journal of Photochemistry and Photobiology A: Chemistry, 170, p. 299-306.
92. Yamazaki, S., Tsukamoto, H., Araki, K., Tanimura, T., Tejedor-Tejedor, I., Anderson, M. A. 2001. Photocatalytic degradation of gaseous

tetrachloroethylene on porous TiO_2 pellets. - Applied Catalysis B: Environmental, 33, p. 109–117.

93. Zhang, F., Zhao, J., Shen, T., Hidaka, H., Pelizzetti, E., Serpone, N. 1998 (a). TiO_2-assisted photodegradation of dye pollutants II. Adsorption and Degradation Kinetics of Eosin in TiO_2 Dispersions under Visible Light Irradiation. - Applied Catalysis B: Environmental, 15, p. 147-156.
94. Zhang, Z., Wang, C.-C., Zakaria, R., Ying, J. Y. 1998 (b). Role of Particle Size in Nanocrystalline TiO_2-Based Photocatalysts. - The Journal of Physical Chemistry B, 102, p. 10871 – 10878.
95. Zhao, J., Yang, X. 2003. Photocatalytic oxidation for indoor air purification: a literature review. - Building and Environment, 38, p. 645 – 654.
96. Zhao, X., Zhao, Q., Yu, J., Liu, B. 2008. Development of multifunctional photoactive self-cleaning glasses. - Journal of Non-Crystalline Solids, 354, p. 1424-1430.
97. Zhong, L., Haghighat, F. 2011. Modeling and validation of a photocatalytic oxidation reactor for indoor environment applications. - Chemical Engineering Science, 66, p. 5945-5954.

ABSTRACT

Photocatalysis is the process, where semiconductor, usually titanium dioxide, activated by light energy initiates electrochemical reactions allowing, for example, to remediate air from indoor pollutants. Hazardous air pollutants aliphatic acrylonitrile (AN) and aromatic toluene were chosen for gas-phase photocatalytic oxidation (PCO) studies.

The objectives of the present research were:

- the estimation of the PCO potential in degradation of gaseous AN and its sensitivity towards reaction conditions,
- the identification of the products of AN PCO and thermal degradation,
- the establishing the potential of sulphated TiO_2 P25 catalyst improving the AN PCO performance,
- the evaluation of the gas-phase photocatalytic activity of the new flame synthesized F3 nano-powder photocatalyst compared to commercial P25 towards AN and toluene.

Carbon dioxide, water and nitrogen dioxide or adsorbed nitric acid were the main products of AN photocatalytic oxidation. Detected gaseous reaction by-products of AN PCO were HCN, N_2O, and CO. The oxidation of HCN to NO_2 and further formation of HNO_3 adsorbed on a photocatalyst' surface in the present of water vapour was followed by means of temperature-programmed oxidation study.

Photocatalytic activity of sulphated-TiO_2 was higher compared to P25 towards the degradation of AN at the longest residence times and at elevated temperature. The temperature decrease had negative effect on the performance of sulphated P25 photocatalyst.

The new flame aerosol synthesized photocatalyst F3 showed the unselective photocatalytic activity exceeding commercial P25 in the degradation of well-adsorbed AN and weekly adsorbed toluene. The process safety required lower operational temperature because of increased desorption of surface hydroxyl groups from F3 surface resulting in the reduced degradation of HCN.

The future of photocatalysis technology for air remediation will be depending to a great extent on the development of effective catalytic materials possessing unselective activity towards volatile organic compounds.

KOKKUVÕTE

Käesolevas töös uuriti levinud õhu saasteainete, akrüülnitriili ja tolueeni, fotokatalüütilist oksüdatsiooni (FKO). Fotokatalüütiline oksüdatsioon on protsess, mille käigus elektromagnetkiirguse toimel katalüsaatori, tavaliselt titaandioksiidi, pinnal toimuvad elektrikeemilised reaktsioonid, mis lubavad näiteks lagundada õhus olevaid saasteaineid. Fotokatalüütilist oksüdatsiooni on edukalt kasutatud paljude orgaaniliste ainete lagundamiseks, kuid kirjandusandmeid akrüülnitriili FKO kohta ei leidu. Samas laialt uuritud tolueeni on võimalik kasutada uute katalüsaatorite efektiivsuse määramiseks.

Uurimistöö eesmärkideks oli:

- Uurida FKO võimet lagundada akrüülnitriili P25 (Degussa/Evonik) titaandioksiidil;
- Selgitada välja katsetingimuste mõju (saasteainete kontsentratsioon, temperatuur, viibimisaeg, niiskus) akrüülnitriili FKO protsessile torureaktoris;
- Uurida akrüülnitriili FKO produkte ja vaheprodukte pideva töörežiimiga torureaktoris ning poolperioodilises reaktoris kasutades temperatuur-programmeeritud oksüdatsiooni meetodit;
- Süstemaatiliselt uurida akrüülnitriili FKO-d sulfateeritud P25 titaandioksiidil ning akrüülnitriili ja tolueeni FKO-d leekaerosoolmeetodiga sünteesitud F3 titaandioksiidil.

Akrüülnitriil oksüdeerub kiiresti FKO käigus. Akrüülnitriili lagundamise põhiproduktid määrati FTIR- ning mass-spektromeetria abil, nendeks on süsinikdioksiid, vesi ja lämmastikdioksiid või titaandioksiidi pinnal adsorbeeritud lämmastikhape. Reaktsiooni vaheproduktideks on vesiniktsüaniid, dilämmastikoksiid ja süsinikoksiid. Termiline oksüdatsioon titaandioksiidi pinnal ilma UV-kiirguseta ja UV-kiirguse all näitas, et HCN võib FKO käigus oksüdeeruda täielikult lämmastikudioksiidini, moodustades vee aurude juuresolekul lämmastikhappe, mis adsorbeerub fotokatalüsaatori pinnale.

Akrüülnitriili FKO läbi viimisel pikema viibimisajaga ja kõrgemal temperatuuril oli sulfateeritud P25-l fotokatalüütiline aktiivsus kõrgem kui tavalisel P25-l. Temperatuuri alandamisel oli sulfateeritud P25 toime tugevalt häiritud.

Uudse leekaerosoolmeetodiga sünteesitud F3 fotokatalüsaatori toime ületab kommertskatalüsaatori P25 toimet nii alifaatse akrüülnitriili kui ka aromaatse tolueeni FKO-l. F3 titaandioksiid omab võrreldes P25-ga kõrgemat oksüdeerimisvõimet, mis väheneb temperatuuri tõusu ja katalüsaatori pinna dehüdrateerimisega.

Fotokatalüüsi tehnoloogia rakendamise tulevik õhu puhastamisel sõltub suurel määral lenduvate orgaaniliste ühendite lagundamiseks kasutatavate mitteselektiivsete fotokatalüsaatorite edasisest sünteesist.

APPENDIX I. PUBLICATIONS

PAPER I

Krichevskaya, M., Jõks, S., Kachina, A., Preis, S. 2009. Gas-phase photocatalytic oxidation of acrylonitrile. - Photochemical and Photobiological Sciences, 8(5), p. 600 - 603.

Reproduced by permission of The Royal Society of Chemistry (RSC) for the European Society for Photobiology, the European Photochemistry Association, and the RSC.

Gas-phase photocatalytic oxidation of acrylonitrile†

Marina Krichevskaya,*[a] Svetlana Jõks,[a] Anna Kachina[b] and Sergei Preis[a,b]

Received 30th September 2008, Accepted 16th January 2009
First published as an Advance Article on the web 28th January 2009
DOI: 10.1039/b817063k

Published on 28 January 2009 on http://pubs.rsc.org | doi:10.1039/B817063K
Downloaded by Tallinn University of Technology on 17 October 2011

Photocatalytic oxidation (PCO) of acrylonitrile (AN) on titanium dioxide in the gaseous phase was studied. AN readily undergoes photocatalytic degradation in a gas–solid system by using TiO_2 Degussa P25. The AN PCO volatile products, visible in the infrared spectra, included nitrogen dioxide, nitrous oxide, carbon dioxide, water, hydrogen cyanide and carbon monoxide. Longer contact time resulted in deeper oxidation of AN with decreasing hydrogen cyanide and increasing nitrogen dioxide content. The effect of temperature increasing from 60 to 130 °C was observed to be slightly negative in terms of AN degradation rate. However, the effect of increased temperature was noticeable in terms of the character and yields of the PCO products: HCN peaks diminished with growing peaks of NO_2.

Introduction

Indoor air quality has become an important community concern due to the increased amount of personnel time spent in indoor environment.[1] Some studies showed that the level of pollutants in indoor environments actually exceeds that of the outdoors.

Many volatile organic compounds (VOCs) are known to be toxic and considered to be carcinogenic, mutagenic, or teratogenic. The Environmental Protection Agency (EPA) original list of hazardous air pollutants includes two nitrile compounds: acrylonitrile CH_2=CHCN (AN) and acetonitrile CH_3CN. Studies have demonstrated that AN can induce gene mutations, chromosome aberrations, unscheduled DNA synthesis and cell transformation.[2] Chronic studies provide convincing evidence that AN is carcinogenic for animals when administered by the inhalation route of exposure. Epidemiologic studies have associated AN exposure in the workplace with increased incidence of lung cancer and possibly prostate cancer.

Population exposure to AN in the environment is small except near factories or waste sites. However, exposure to AN can also occur from residual AN in commercial fibrous polymeric material, usually less than 1 mg kg^{-1}, in resins, about 30–50 mg kg^{-1}, and in styrene–acrylonitrile resins, about 15 mg kg^{-1}; concentrations in rubber and latex vary widely.[2] Relatively large amounts are liberated by fires. AN also has been detected in cigarette smoke as 3 to 15 mg per cigarette, and in commercial acrylamide, 25–50 mg kg^{-1}.[3,4] The health authorities of the Federal Republic of Germany have placed AN in the category of carcinogenic chemicals for which no threshold limits are established. The US EPA has classified AN as a "water priority pollutant" and a "hazardous air pollutant".

Because of the limitations of traditional end-of-pipe techniques, like absorption and adsorption methods, thermal and catalytic incineration and biotechnological abatement methods the development of an alternative remediation technology such as heterogeneous photocatalytic oxidation (PCO) is a research challenge.

Photocatalytic processes are based on the absorption of UV radiation by the semiconductor photocatalyst with further oxidation of adsorbed organic molecules. The final result can be, under favourable conditions, the complete mineralisation of organic pollutants.

The objective of the present research was to estimate the PCO potential in degradation of gaseous AN and its sensitivity towards reaction conditions as well as to disclose routes of AN degradation. The declared objective was achieved by experimental research undertaken into the PCO of AN dependently on concentration of pollutant, its residence time, air humidity and temperature. The identification of volatile PCO products was also carried out. Deactivation of the photocatalyst and restoration of its activity was also taken under consideration.

Results and discussion

PCO by-products of AN

Fig. 1 shows the infrared spectra of AN PCO gaseous products obtained at AN inlet concentration 40 ppmv, 130 °C, relative humidity (RH) 0%, and residence time 6.4 s.

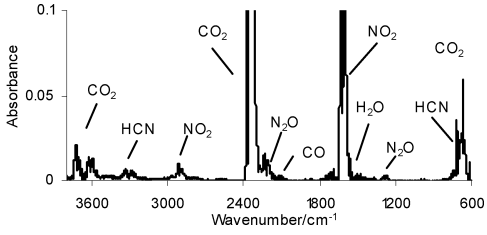

Fig. 1 FT-IR spectrum of the outlet flow containing PCO products of AN.

[a]*Department of Chemical Engineering, Tallinn University of Technology Ehitajate tee 5, 19086, Tallinn, Estonia. E-mail: marina.kritsevskaja@ttu.ee; Fax: +372 620 2856; Tel: +372 620 2857*
[b]*Department of Chemical Technology, Lappeenranta University of Technology, P.O. Box 20, 53851, Lappeenranta, Finland; Fax: +358 5621 2199; Tel: +358 5621 2103*

† This paper was published as part of the themed issue of contributions from the 5th European Meeting on Solar Chemistry and Photocatalysis: Environmental Applications held in Palermo, Italy, October 2008.

 This journal is © The Royal Society of Chemistry and Owner Societies 2009

Downloaded by Tallinn University of Technology on 17 October 2011
Published on 28 January 2009 on http://pubs.rsc.org | doi:10.1039/B817063K

The AN PCO volatile products, visible in the infrared spectra, included nitrogen dioxide, nitrous oxide, carbon dioxide, water, hydrogen cyanide and carbon monoxide. Longer contact time resulted in deeper oxidation of AN with decreasing hydrogen cyanide peaks and increasing in peaks of nitrogen dioxide.

During the PCO studies of another nitrile compound, the acetonitrile, it was found that carbon dioxide and hydrogen cyanide were the main products of acetonitrile degradation.[5] The moles of cyanide ions and of produced CO_2 corresponded to those of acetonitrile degraded. In other studies of PCO of acetonitrile the authors claimed the breaking of the acetonitrile C–C bond and proposed a reaction mechanism where the principal products were CO_2 and N_2.[6] On the TiO_2 surface they observed isocyanate species, subsequently transformed to CO_2 and N_2; nitrogen was proposed, but not observed by analytic technique. The authors did not observe hydrogen cyanide, probably because this compound was not present in adsorbed phase but was released to the gas phase.

Differently from the results of those works, CO_2 and NO_2 were observed as the main products of the PCO of AN. There could be supposed a two step mechanism involving initially the PCO of the CH_2=CH– moiety to CO_2 in adsorbed CH_2=CHCN. PCO of CN moiety liberated by the first step of oxidation leads to formation of nitrogen dioxide NO_2. Formation of nitrous oxide N_2O was described as a result of PCO of ammonia in the presence of nitrogen oxide NO.[7] Nitrogen oxide presumably formed in the PCO reaction from ammonia, was partially oxidized further to nitrogen dioxide and partially reacted with residual ammonia forming nitrous oxide. Ammonia was not seen among the AN oxidation products at shorter residence times (from 3.2 to 6.4 s) supposedly due to small amounts of ammonia formed. Infrared spectra obtained for the longest residence time 12.8 s showed some peaks at 900–1000 cm^{-1} range, which may be attributed to ammonia or AN. Peaks of initial pollutant AN observed in this range in FT-IR spectra, disappeared much earlier, already at residence time 6.4 s, and cannot interfere at 12.8 s. Therefore, we have indirect proof of ammonia formation among AN PCO by-products, although ammonia was not pronouncedly seen among the gaseous products in FT-IR spectra.

The observed CN moiety exhibits the behaviour expected for an intermediate species, leading to the final oxidation of the CN moiety with increase in temperature or/and longer residence time (see also Effect of temperature).

The oxidation of CH_2=CH– moiety to CO_2 apparently involves formation of oxygenated by-products readily oxidised or dimers or polymers leading to deactivation of the photocatalyst. The formation of CO could be attributed to the formation of carbonyl groups.[8] The formation of carbonaceous species (dimers, polymers) on the surface of the TiO_2 catalyst was also observed during PCO of unsaturated organic compounds.[9]

Effect of residence time and pollutant concentration

The PCO of AN was examined at various contact times. The dependence of the conversion values of AN ($(C_{in} - C_{out})/C_{in}$ or $1 - C_{out}/C_{in}$, %) on different inlet concentrations and residence time in reactor is shown in Fig. 2(a) and (b)

The increase in the residence time up to 6.4 s resulted in a growth of AN PCO conversion at all concentrations.

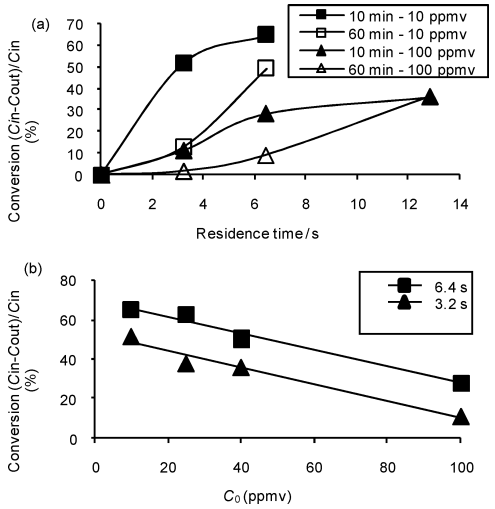

Fig. 2 (a) Effect of residence time on the AN degradation after 10 and 60 min of continuous run: AN inlet concentration 10 and 100 ppmv, RH 0%, 130 °C. (b) Dependence of AN degradation on AN initial concentration at different residence times: RH 0%, 130 °C, reaction time 10 min.

The AN conversion degree increased with residence time, although not linearly. Experiments at longer residence time up to 12.8 s resulted in inadequate measurements due to interference of oxidation by-products, which absorbed in the same IR spectrum range as AN. Alterations were observed with all AN inlet concentrations excluding 100 ppmv. This could be explained with small amounts of by-products formed at runs with high AN inlet concentrations. The complex mechanism of photocatalytic reactions including adsorption of the target compound followed by oxidation of adsorbed species, oxidation of by-products formed and desorption of by-products and unreacted initial compounds may explain the non-linear increase in AN conversion with residence time by, for example, the slowdown in desorption processes and therefore retardation of adsorption of AN.

The poisoning of the photocatalyst was observed during PCO of AN at all inlet concentrations and residence time of less than 12.8 s at 130 °C. For example, at 130 °C the degradation of AN at initial concentration of 10 ppmv in dry air with residence time 3.2 s decreased from 51.6% to 12.9% in 1 h from the start of the continuous run. The photocatalyst changed colour from white to different shades of yellow. This indicates that some species adsorbed on the photocatalyst surface during PCO of AN and caused the deactivation. Thus, the rate-limiting stage for AN complete oxidation is the PCO of the adsorbed oxidation intermediates. The degradation rates of the intermediates seem to be slower than the degradation rate of AN.

During PCO of AN at all inlet concentrations up to 100 ppmv and residence time of more than 12.8 s at 130 °C no poisoning of the photocatalyst was observed for 1 h of continuous run, the degradation percent of AN remained the same during this time showing no catalyst deactivation.

Experiments with different inlet concentrations of AN (10, 25, 40 and 100 ppmv) were performed. As shown in Fig. 2(b) the

Downloaded by Tallinn University of Technology on 17 October 2011
Published on 28 January 2009 on http://pubs.rsc.org | doi:10.1039/B817063K

percent conversion of AN during PCO decreased as the VOC inlet concentration increased at residence times 3.2 and 6.4 s. Because intermediates form on the surface and their appearance depends on their rates of formation, desorption, oxidation rate and displacement by other species the reactions are neither first-order nor diffusion-controlled. This indicated that the rate of the process limited by a surface reaction with an order greater than one would be dependent on the AN concentration.

Effect of humidity

Fig. 3(a) shows that the presence of humidity, RH 66% at 130 °C, do not cause alterations in the degradation rate of the AN in 10 min from the start of the experiments at small inlet concentrations of AN (10 and 40 ppmv). A slight decrease in AN conversion was observed at high (100 ppmv) AN concentration in presence of water vapour. The decrease in the PCO rate in the presence of humidity may be explained by the competitive adsorption of water and VOC molecules on the photocatalyst surface.

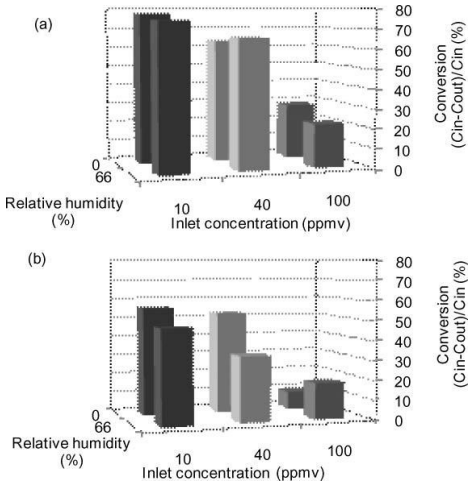

Fig. 3 Effect of humidity on photocatalytic degradation of the AN: (a) 10 min from the start of the run; (b) 60 min from the start of the run (residence time 6.4 s, 130 °C).

After 1 h of continuous run (Fig. 3(b)), the dual effect of water vapour was observed. At small inlet concentrations of AN the decrease in degradation from 10 to 20% compared to dry air was observed. On the contrary, the degradation of AN with an initial concentration of 100 ppmv in 1 h was higher in humid air: the conversion of AN in dry air dropped approximately for 19% (Fig. 3), while in humid air it decreased for only 4%, thus showing the favourable effect of water vapour extending the photocatalyst deactivation time at higher AN concentrations. The durability factor[10] defined here as the ratio of the AN degradation fractions at 1 h to those at the first 10 min, increased with an increase in relative air humidity from 0.32 to 0.83 at AN inlet concentration of 100 ppmv.

An important role of water vapour in the regeneration of the photocatalyst was seen: entire restoration of the photocatalyst activity was achieved by 2 h PCO of adsorbed oxidation by-products in humid airflow, the colour of the photocatalyst turned from yellowish to white. UV-irradiation of the photocatalyst layer in dry air did not restore the photocatalyst's activity; even the colour of the photocatalyst remained yellow.

Effect of temperature

Temperature is one of the most important factors in gas–solid heterogeneous reactions. Photoctalytic reactions, however, are not sensitive to minor variations in temperature.[11] This is explained by the fact that at low temperature, desorption of the products from the photocatalyst surface is the rate determining step, whereas at higher temperatures adsorption of reactants becomes the rate determining step.

The minor negative effect of increasing temperature from 60 to 130 °C was observed after 10 min of PCO and after 1 h of continuous run. However, a noticeable effect of temperature on the PCO of AN was observed in the character and quantities of the AN PCO products. Fig. 4 shows the infrared spectra of hydrogen cyanide and nitrogen dioxide—the gaseous products of PCO of AN at 60 and 130 °C.

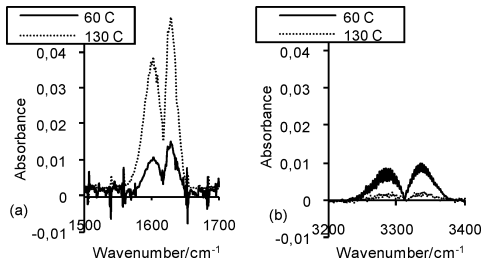

Fig. 4 The infrared spectra of AN products at 60 and 130 °C: (a) nitrogen dioxide and (b) hydrogen cyanide (inlet AN concentration 30 ppmv, RH 0%, residence time 6.4 s).

One can see the evolution of the AN PCO products with increasing temperature, the growth of nitrogen dioxide peaks at the IR bands from 1550 to 1650 cm^{-1} and the decrease of hydrogen cyanide peaks at the IR bands from 3200 to 3400 cm^{-1}: higher temperature resulted in deeper oxidation of AN showing more profound oxidation of hydrogen cyanide and therefore the higher yield of nitrogen dioxide.

Experimental

TiO_2 powder was obtained from Degussa AG (P-25). Concentration of gaseous AN (Sigma-Aldrich, ≥99.5%) varied from 10 to 100 ppmv.

The gas-phase PCO of AN over UV-illuminated TiO_2 was studied using an annular photocatalytic reactor having an inner diameter 33 mm and total volume of 0.105 L used in a continuous gas-flow mode. The annular gap between the lamp and the inner wall of the reactor was 3.5 mm. A 365 nm 15 W low-pressure mercury luminescent UV-lamp was positioned coaxially in the reactor. The reactor was coated inside with TiO_2 by rinsing 50 times with a TiO_2 aqueous suspension, each rinse followed by drying. This made the TiO_2 coverage in the reactor 1.4 mg cm^{-2} and the total mass of the photocatalyst 0.9 g. Before the experiments the

 This journal is © The Royal Society of Chemistry and Owner Societies 2009

reactor was washed by liquid 50% H_2O_2. At the end of each run, the photoreactor was treated by water vapour to restore photocatalyst activity for 2 h and then was dried at 120 °C for 2–3 h.

The irradiance of the TiO_2-coated UV-lamp was measured with a UVX Radiometer at the surface next to the lamp and average about 0.6 mW cm^{-2}.

The equipment consists of a thermostatted reactor, gas flow controllers, gas humidifier and Wilks MIRAN 1A infrared analyzer. The gas samples for the reaction products analysis by means of FT-IR (Perkin Elmer 2000, Lappeenranta University of Technology) were collected to a Sirocco 10.6 m gas cell.

The temperature in the reactor was maintained within a range of 60 to 130 °C. The gas flow controllers provided gas flow rates from 0.2 to 2.0 L min^{-1}. The in-line humidifier allowed the RH in the gas stream to be maintained from 0 to about 70% determined at 20 °C.

The VOC feed tank was charged with polluted air by tank evacuation and injection of a pollutant (AN) through the injection port. Then the tank was charged with compressed air (3 atm). Time for vacuum evaporation was 10 min and time for mixing was 24 h.

The diluent feed tank was used to dilute the polluted gas stream with the carrier gas—dry or humidified air.

The run procedure was the same through the study. The runs lasted 60 min, and the gas leaving photoreactor was analyzed every 10 min. Each experiment was repeated two or three times, arithmetic mean values are presented in figures and tables.

Conclusions

The photocatalytic degradation of AN successfully occurs in gas–solid systems by using TiO_2 Degussa P25. The main reaction products were CO_2, H_2O and NO_2; the intermediate products HCN, N_2O and CO were observed. These findings suggest breakage of the AN C–C bond. Longer contact time resulted in deeper oxidation of AN.

The AN conversion values increased with residence time, although not linearly. At longer residence time up to 12.8 s resulted in inadequate measurements due to interference of oxidation by-products, which absorbed in the same IR spectrum range as AN, possibly ammonia.

The poisoning of the photocatalyst was observed during PCO of AN at all inlet concentrations and residence time of less than 12.8 s at 130 °C. However, within the AN concentration limits used in experiments (up to 100 ppmv) no photocatalyst deactivation was observed at 130 °C and 12.8 s residence time.

The presence of water vapour did not affect the degradation rate of AN within the first 10 min from the start of the experiments at 130 °C. However, after 1 h of continuous run, a dual effect of water vapour was observed. At relatively small inlet concentrations, up to 40 ppmv, the AN degradation rate decreased from 10 to 20% compared to dry air. On the contrary, at higher AN concentrations, about 100 ppmv, the presence of water vapour alleviated the photocatalyst deactivation. An important role of water vapour in the regeneration of the photocatalyst was also seen: entire restoration of the photocatalyst activity was achieved by 2 h PCO of adsorbed oxidation by-products in humid airflow.

The effect of temperature increasing from 60 to 130 °C was observed to be slightly negative in terms of AN degradation during 1 h of continuous run. However, the effect of increased temperature was noticeable in terms of the character and yields of the PCO products: HCN content diminished with growing content of NO_2.

Acknowledgements

The authors gratefully acknowledge support by the Estonian Science Foundation (Grant 7541).

Notes and references

1 S. Wang, H. M. Ang and M. O. Tade, Volatile organic compounds in indoor environment and photocatalytic oxidation: State of the art, *Environ. Int.*, 2007, **33**, 694–705.
2 A. Léonard, G. B. Gerber, C. Stecca, J. Rueff, H. Borba, P. B. Farmer, R. J. Sram, A. E. Czeizel and I. Kalina, Mutagenicity, carcinogenicity, and teratogenicity of acrylonitrile, *Mutat. Res.*, 1999, **436**, 263–283.
3 G. D. Byrd, K. W. Fowler, R. D. Hicks, M. E. Lovette and M. F. Borgerding, Isotope dilution gas chromatography-mass spectrometry in the determination of benzene, toluene, styrene and acrylonitrile in mainstream cigarette smoke, *J. Chromatogr.*, 1990, **503**, 359–368.
4 G. Scherer, J. Engl, M. Urban, G. Gilch, D. Janket and K. Riedel, Relationship between machine-derived smoke yields and biomarkers in cigarette smokers in Germany, *Regul. Toxicol. Pharmacol.*, 2007, **47**, 171–183.
5 V. Augugliaro, S. Coluccia, E. Garćia-López, V. Loddo, G. Marci, G. Martra, L. Palmisano and M. Schiavello, Comparison of different photocatalytic systems for acetonitrile degradation in gas–solid regime, *Top. Catal.*, 2005, **35**, 237–244.
6 J. Zhuang, C. N. Rusu and J. T. Yates, Adsorption and photooxidation of CH_3CN on TiO_2, *J. Phys. Chem. B*, 1999, **103**, 6957–6967.
7 A. Kachina, S. Preis, G. C. Lluellas and J. Kallas, Gas-phase and aqueous photocatalytic oxidation of methylamine: the reaction pathway, *Int. J. Photoenergy*, 2007, DOI: 10.1155/2007/32524.
8 S. A. Larson and J. L. Falconer, Initial reaction steps in photocatalytic oxidation of aromatics, *Catal. Lett.*, 1997, **44**, 57–65.
9 C. T. Brigden, S. Poulston, M. V. Twigg, A. P. Walker and A. J. J. Wilkins, Photo-oxidation of short-chain hydrocarbons over titania, *Appl. Catal. B*, 2001, **32**, 63–71.
10 H. Einaga, S. Futamura and T. Ibusuki, Heterogeneous photocatalytic oxidation of benzene, toluene, cyclohexene and cyclohexane in humidified air: comparison of decomposition behaviour on photoirradiated TiO_2 catalyst, *Appl. Catal. B*, 2002, **38**, 215–225.
11 S. B. Kim and S. C. Hong, Kinetic study for photocatalytic degradation of volatile organic compounds in air using thin film TiO_2 photocatalyst, *Appl. Catal. B*, 2002, **35**, 305–315.

Downloaded by Tallinn University of Technology on 17 October 2011
Published on 28 January 2009 on http://pubs.rsc.org | doi:10.1039/B817063K

PAPER II

Jõks, S., Krichevskaya, M., Preis, S. 2011. Gas-phase photocatalytic oxidation of acrylonitrile on sulphated TiO_2: continuous flow and transient study. - Catalysis Letters, 141(2), p. 309 - 315.

Reprinted with the permission from the Springer Science+Business Media, LLC.
© Springer

Catal Lett (2011) 141:309–315
DOI 10.1007/s10562-010-0501-2

Gas-phase Photocatalytic Oxidation of Acrylonitrile on Sulphated TiO_2: Continuous Flow and Transient Study

Svetlana Jõks · Marina Krichevskaya · Sergei Preis

Received: 5 October 2010 / Accepted: 9 November 2010 / Published online: 24 November 2010
© Springer Science+Business Media, LLC 2010

Abstract The gaseous products of photocatalytic oxidation (PCO) of acrylonitrile on sulphated P25 in concentrations from 10 to 100 ppm at 60 to 130 °C were CO_2, HCN and HNCO. This photocatalyst showed disproportionally improved performance at higher temperature and longer retention times. The temperature-programmed oxidation (TPO) after PCO disclosed possible reaction routes.

Keywords 2-Propenenitrile · Photocatalytic oxidation · Thermal degradation · Sulphated titanium dioxide · Air pollution

1 Introduction

The hazardous air pollutants include acrylonitrile (AN) CH_2=CH–CN exhibiting mutagenic, carcinogenic and teratogenic properties [1]. This volatile organic compound (VOC) is detected as an in-door air component emitted by commercial fibrous polymeric materials, resins and smoking tobacco [2, 3]. Traditional VOCs control technologies include adsorption [4], thermal incineration at temperatures of 1000–1200 °C, catalytic incineration at temperatures of 250–500 °C [5–7] and bio-filtration [8–10] suffering from high operating costs, secondary waste stream problems and narrow range of working conditions (bio-filtration).

The problem of emerging pollution of the atmosphere with VOCs and their insufficient or costly abatement strategies necessitate the search for effective alternatives. One of the methods of cleaning air from various VOCs in dilute concentrations is photocatalytic oxidation (PCO) employing a UV-irradiated semiconductor catalyst, usually TiO_2: the method has oxidation potential sufficient to oxidize the widest spectrum of pollutants at near-ambient temperature using direct solar energy. The general drawbacks of PCO, such as low reaction rates and the catalyst poisoning, require relevant improvement to expand PCO application area. A potentially cost-effective way to improve the photocatalysts performance is increasing the number and the adsorption capacity of surface acid sites since PCO activity has been shown to increase with catalyst surface acidity [11, 12]. Sulphated metal oxides are particularly effective acid catalysts [13–15], indicating a promising way of development.

The sulphate ion forms S=O and O–S–O bonds in TiO_2, creating unbalanced charge on Ti-atoms, vacancies and defects in the titania structure [16]. In sulphated titanium dioxide, the O=S=O group anchored to the surface seems to trap electrons improving the oxidation process, retarding the recombination of holes and electrons induced by UV irradiation. The O=S=O species polarize the S=O bonds in presence of water to coordinate its molecules, giving an anchored sulphate, in which sulphur electron-deficient species are induced [17].

The preliminary results of PCO of AN vapours on TiO_2 P25 were described briefly in the recent publication [18]. The present study uses both transient and continuous-flow methods for disclosing the PCO mechanism for AN. The PCO reaction can be started and stopped by turning the UV

S. Jõks · M. Krichevskaya (✉)
Department of Chemical Engineering, Tallinn University of Technology, Ehitajate tee 5, 19086 Tallinn, Estonia
e-mail: marina.kritsevskaja@ttu.ee

S. Jõks
e-mail: lanka@starline.ee

S. Preis
LUT Chemistry, Lappeenranta University of Technology, P.O. Box 20, 53851 Lappeenranta, Finland
e-mail: sergei.preis@lut.fi

lights on and off in transient studies combined with the mass-spectrometry. The adsorbed intermediates may be subsequently identified in temperature-programmed oxidation (TPO) also combined with the mass-spectrometry [19]. Also TPO is an important tool for characterizing of used catalysts and their regeneration [20].

The major advantage of PCO is the reaction at room-temperature. The geometry of photocatalytic reactors, however, is supposed to optimise utilization of light by bringing the irradiated photocatalyst surface sufficiently close to the source of radiation, usually the mercury UV lamp, thus increasing the temperature of treated gas. For example, in the present study the working low-pressure Hg-lamp maintained the temperature in the reactor from 60 to 130 °C dependent only on the insulation of reactor. The PCO reaction rate depends on temperature on account of adsorption, reaction kinetics, and desorption of products. Higher temperature accelerates the reaction and makes the removal of reaction products from the photocatalyst surface easier [21], providing more active sites for PCO reaction and thus extending the photocatalyst activity, while low temperature is beneficial for adsorption. The interaction of these trends results in a variety of the PCO performance, oxidation products and the catalyst stability at various temperatures.

The current study was focused on the identification of the products of AN thermal degradation and PCO obtained on the course of the transient and the continuous-flow study, as well as on the effects of temperature and the potential of sulphated TiO_2 P25 catalyst to improve the AN PCO performance.

2 Experimental

2.1 Transient PCO

A thin-film annular reactor was used for transient PCO [22]. The catalyst, Degussa P25, was coated onto the Pyrex glass by rinsing it for 50 times with the photocatalyst aqueous suspension with each rinse followed by drying. This photoreactor consists of two concentric Pyrex cylinders that form an annular region with a 1 mm gap. The outer diameter of the inner cylinder is 20 mm, and the height—160 mm. The total mass of the photocatalyst deposited in the reactor was 0.4 g making the TiO_2 coverage 1.9 mg cm^{-2}. The reactor was surrounded by a UV-transparent furnace, and twelve 8 W "black light" UV-tubes (BLB Korea, type F8T5BLB), placed in a circle at a distance of 6 cm from the reactor for the reactor irradiation. Radiometer measurements showed a UV intensity of 2.5 mW cm^{-2} and a maximum light intensity at 360 nm [23]. The gas-phase species in the outlet stream were analysed by a quadrupole mass spectrometer (Balzers, QMA 125).

The PCO reaction in transient mode can be started and stopped by turning the UV radiation on and off to have adsorbed intermediates identified by TPO subsequent to PCO; the temperature was increased at a constant rate of 1 K s^{-1}. Heating was stopped at 400 °C to avoid irreversible changes in the TiO_2 structure from anatase to rutile. PCO and TPO of AN were carried out in 20% O_2–80% He mixture flow (120 standard cm^3 min^{-1}).

Before each experiment, the catalyst was heated to 400 °C in the O_2/He flow to obtain a reproducible oxide surface. The UV-lights were turned on and allowed to warm up for approximately 15 min before the cover over the reactor was removed to start the reaction. Acrylonitrile was adsorbed onto the catalyst by its injecting into the gas stream at the top of the reactor at three different temperatures of 50, 90 and 130 °C. The amounts of the AN injected were 0.1, 0.2 and 0.5 μl constituting the AN concentration of 20, 40 or 100 ppm referred to the volume of photocatalytic reactor. This was to observe the impact of the AN concentration to the character of the PCO by-products.

Each transient PCO run was carried out in three ways: (a) dark adsorption at temperature of 50, 90 or 130 °C followed by dark TPO, (b) PCO at the specified temperature followed by dark TPO and (c) PCO at specified temperature followed by TPO with the UV lights being constantly switched on during the PCO and TPO.

2.2 Continuous-Flow Mode

The experimental equipment consists of a thermostatted reactor, gas flow controllers and INTERSPEC 200-X FTIR spectrometer with the Specac Tornado 8-m 1.33-l gas cell with ZnSe-windows. The annular photocatalytic reactor having an inner diameter 33 mm and total volume of 0.105 l was used in a continuous gas-flow mode. A 365 nm 15 W low-pressure mercury luminescent UV-lamp was positioned coaxially in the reactor. The annular gap between the lamp and the inner wall of the reactor was 3.5 mm. The reactor's inner surface and the lamp were coated with sulphated TiO_2 using the same procedure as for reactor used in transient mode. TiO_2 P25 was obtained from Degussa AG and treated with H_2SO_4 by the method described in [24]. The total mass of the photocatalyst in the reactor was 1.3 g and thus the catalyst coverage was 2.0 mg cm^{-2}. The irradiance of the TiO_2-coated UV-lamp was measured with a UVX Radiometer at the surface next to the lamp averaging 0.64 mW cm^{-2}.

The VOC feed tank was charged with polluted air by tank evacuation and injection of AN through the injection port. After 10 min of evaporation, the tank was pressurised

with compressed air to 3 to 4 bar and left for the concentration balancing overnight. The diluent feed tank was used to dilute the polluted gas stream with the carrier gas, dry air. The gas flow controllers provided gas flow rates from 0.5 to 2.0 l min^{-1}. The runs lasted for 60 min with the continuous FT-IR outlet gas analysis. The concentration of AN (Sigma-Aldrich, ≥99.5%) vapours varied from 10 to 100 ppm. The temperature in the reactor was maintained within a range from 60 to 130 °C controlled by the heating tape with the temperature controller.

3 Results and Discussion

3.1 Transient PCO and TPO Studies

3.1.1 Transient PCO

Acrylonitrile readily reacted on the UV-irradiated TiO_2 catalyst to form carbon dioxide as the main gas-phase product. As shown in Fig. 1 (a), carbon dioxide formed immediately after the AN injection into the irradiated transient PCO reactor (about 60 s after the start of data acquisition). Carbon dioxide formation quickly dropped to zero when the UV lights were turned off. To follow the desorption and thermal degradation of AN at corresponding temperatures, dark adsorption runs were carried out similarly: the AN injection to the reactor in dark was monitored (Fig. 1b). No AN desorption or thermal degradation was seen at 50 °C. At 90 °C the thermal degradation was minor and slow: slight AN desorption along with carbon dioxide and HCN formation were observed in about 180 s after AN injection. At 130 °C, however, the immediate desorption of AN along with its partial thermal degradation was seen: all three peaks of AN, HCN and CO_2 were seen instantly after the injection. Photocatalytic oxidation (Fig. 1a) of injected AN resulted in no AN desorbed at any concentration or temperature within about 10 min of irradiation. No gaseous products other than carbon dioxide were observed in AN PCO at temperatures below 130 °C. The HCN product was seen only at 130 °C at the AN relative concentration as high as 100 ppm; the levels of HCN concentrations much lower than for dark adsorption were seen. Relative concentrations of 20 and 40 ppm are not shown on the Fig. 1 since no desorption of AN or its thermal degradation products, as well as no other gaseous PCO products besides CO_2, were seen at any temperature.

3.1.2 Transient TPO

In Fig. 2 the peak areas of desorbed AN during TPO from the starting temperature, i.e. 50, 90 or 130 to 400 °C were

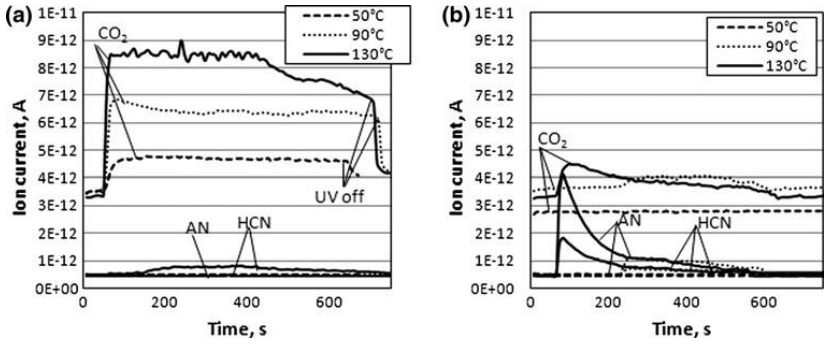

Fig. 1 Transient photocatalytic oxidation (**a**) and desorption/thermal oxidation (**b**) of AN on TiO_2 P25 at different catalyst temperatures: AN concentration 100 ppm

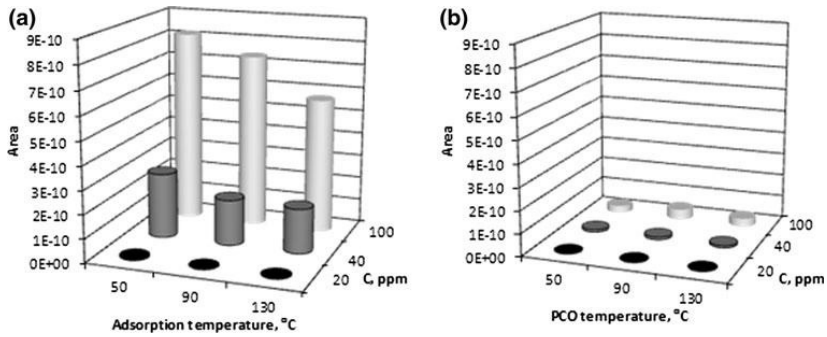

Fig. 2 Temperature programmed oxidation of AN: AN desorption mass spectra peaks area after dark adsorption (**a**), and after 10-min PCO (**b**)

plotted after the AN dark adsorption (Fig. 2a) and after its 10-min PCO (Fig. 2b). One can see that PCO leads to practically total degradation of initial compound at lower AN concentrations (Fig. 2b). The effectiveness of PCO found also a proof in the UV–TPO after PCO (not shown), where no desorbed AN was detected at any temperature and amounts adsorbed. The smaller desorption of AN with TPO observed at higher adsorption temperatures is due to the partial AN desorption and thermal degradation (Figs. 2a, 1b).

The study of the AN thermal oxidation products was carried out more thoroughly with the highest AN relative concentration of 100 ppm. The AN TPO products after the AN dark adsorption, i.e. AN thermal degradation products in presence of oxygen varied slightly with temperature (Fig. 3). At lower temperatures of approximately 90–110 °C the desorption of CO_2, CO, H_2O and HCN started. Species like CH_3CH_2– as well as the simplest carbonyl compounds could be assumed to be present in gaseous phase due to the mass spectra data. At higher temperatures, at about 250 to 300 °C the AN thermal degradation products like NH_3, CH_3CN and low levels of NO_2 were observed. The possible pathway of formation of ammonia from AN is hydrolysis of nitrile through the formation of amide group as intermediate and finally formation of ammonia due to the presence of water as thermal degradation product [25]. Thus, the AN thermal degradation products mainly contain nitrogen at the same oxidation state as in the initial compound: only trace amounts of oxidised nitrogen were seen.

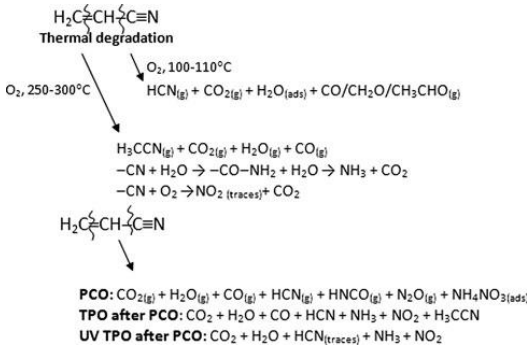

Fig. 3 Outline of thermal degradation and photocatalytic oxidation reactions of gaseous AN

The desorption of the original compound and its PCO products in TPO takes place simultaneously with their thermal degradation (Fig. 4): the gaseous AN thermal degradation products, not all of which are shown at the TPO spectra, were CO_2, CO, H_2O, acetonitrile, HCN, NH_3, NO and NO_2. The TPO spectra of the AN PCO products varied with the AN initial concentration. The desorption of HCN, typical for AN thermal decomposition, started slowly at about 90 °C with higher AN initial concentration (100 ppm) and at about 250 °C with lower AN initial relative concentrations (20 or 40 ppm, see Fig. 4b) increasing steadily up to 350 °C. Nitrogen dioxide (Fig. 4b) and water (Fig. 4a) released starting at about 300 °C may be attributed to the thermal degradation of adsorbed nitric acid as the AN PCO by-product. One can see from Fig. 4b, that some thermal desorption of the residual AN also takes place. No desorbed AN was seen only in TPO combined with UV-irradiation.

Along with the residual AN desorption, the acetontirile desorption at temperatures over 300 °C is observed (Fig. 4b) under all experimental conditions with the exception of UV-TPO series of experiments indicating acetonitrile to be solely the thermal decomposition product.

The emissions of hydrogen cyanide and nitrogen dioxide had the opposite trend during AN TPO. The degradation of cyanide took place during PCO of AN with lower amounts of HCN desorbed at higher temperatures and no HCN was observed during UV-TPO at the lowest AN initial concentration and elevated temperature. On the contrary, ultimate AN PCO products, like nitrogen dioxide, carbon dioxide and water tended to accumulate during PCO and UV-assisted TPO. Cyanide thus appears to be the product of both PCO and thermal decomposition of AN: the amount of HCN desorbed after 10-min PCO is noticeably bigger than could be expected from the amount of desorbed residual AN available after PCO (Fig. 2b).

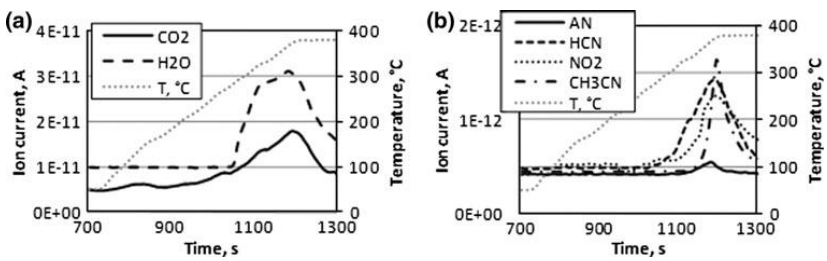

Fig. 4 TPO after 10-min PCO of AN (50 °C, AN concentration 40 ppm): **a** carbon dioxide and water, **b** AN, hydrogen cyanide, nitrogen dioxide and acetonitrile

3.2 Continuous-Flow PCO of AN with Sulphated TiO_2

3.2.1 PCO by-Products

Figure 5 shows the infrared spectra of AN PCO volatile products obtained over sulphated TiO_2 at AN inlet concentration of 100 ppm, 130 °C and retention time of 12.8 s in dry air including nitrous oxide N_2O, carbon dioxide, water, hydrogen cyanide, carbon monoxide and traces of isocyanic acid HNCO.

The products formed on sulphated TiO_2 differ from the ones formed on Degussa P25 [18] in part of HNCO, the peaks of which appear in the volatile products spectra (Fig. 5). The kinetics and the products of the gas-phase reaction between atomic oxygen and HCN have been examined in several studies: HNCO intermediate is formed by rearrangement of oxazarine, the product of oxygen addition to HCN (Reaction 1) [26]. The HNCO is known to hydrolyse in presence of water molecules forming ammonia and CO_2 [27], which explain its minor appearance in the outlet stream.

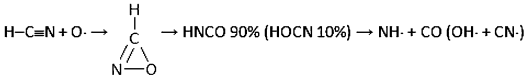

1

Another difference in behaviour of the catalysts was in nitrogen dioxide, clearly seen at PCO of AN on Degussa P25 and not observed with sulphated catalyst. Due to the presence of water as the AN PCO by-product, the formation and adsorption of nitric acid and ammonium ions on the acidic surface of the sulphated P25 is thus presumed. The following reaction pathway for the PCO of nitrogen-containing compounds was proposed by [28] (Reaction 2):

$$HNO_{3(ads)} + NH_3 \rightarrow NH_4NO_{3(ads)} \rightarrow N_2O + H_2O + HNO_3 + N_2 \quad (2)$$

and [29] showed that the N_2O formation occurs as a result of decomposition of hyponitrous acid (Reaction 3), which in turn forms in oxidation of ammonia with OH-radical:

$$NH_3 + OH^{\bullet} + O_2 \rightarrow HNO \rightarrow N_2O + H_2O \quad (3)$$

Also, formation of nitrous oxide N_2O, observed among the products, was described as a result of PCO of ammonia in the presence of nitrogen oxide NO [30]. This suggests the nitrile group transformation also through the nitrogen oxide. The absence of the catalyst deactivation with nitric acid confirmed in this work was earlier reported by [28].

3.2.2 The Impact of Temperature and Residence Time on PCO Performance

The PCO of AN with sulphated P25 was examined at various contact times. The dependence of the conversion of AN ($\frac{Cin-Cout}{Cin}$ or $1-\frac{Cout}{Cin}$, %) on the inlet concentration and retention time is shown in Figs. 6 and 7.

The continuous flow PCO performance exhibited similar behaviour with both sulphated and plain P25: the maximum conversions were reached at about 30 min after the start of the experimental run, although at the maximum residence time studied the sulphated catalyst showed the conversion almost two times exceeding the one of P25 (Fig. 6). The increasing performance of the catalysts along with the experimental run time may be explained by the accumulation of the reaction products possibly catalyzing the AN PCO reaction. This observation found also a logical support in the dependence of the sulphated catalyst performance on the retention time (see below): the disproportional growth of the conversion rate with the retention time may be explained by the change in the reaction pathway and, thus, kinetics and adsorption/desorption equilibrium. Poor adsorption properties of the sulphated catalyst surface reported previously [12, 15, 24] may contribute to poor performance at shorter retention times.

The photonic efficiencies were calculated [31] for both P25 and sulphated P25 at experiment run time of 30 min, reactor residence time of 12.8 s and temperature 130 °C as

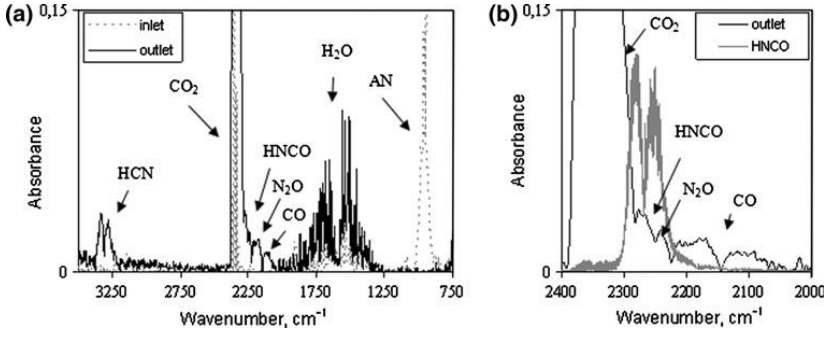

Fig. 5 FT-IR spectrum of the AN inlet (*dashed line*) and outlet (*solid line*) flow containing products of PCO on sulphated TiO_2 (**a**) in the end of 60 min run; the enlarged view allows detection of HNCO (**b**): inlet AN concentration 100 ppm, 130 °C, retention time 12.8 s. HNCO spectrum received by courtesy of Prof. Noel W. Cant, Macquarie University, Australia

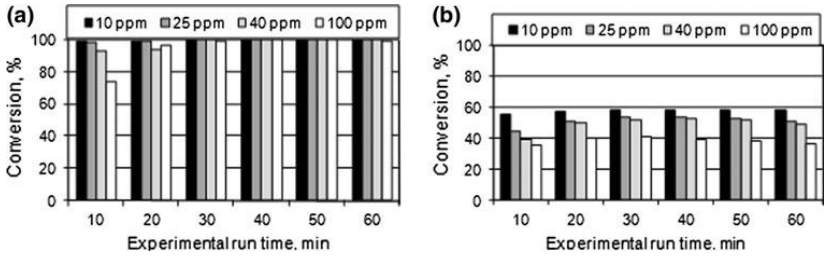

Fig. 6 PCO performance of sulphated (**a**) and plain P25 (**b**) in AN oxidation: 130 °C, retention time 12.8 s

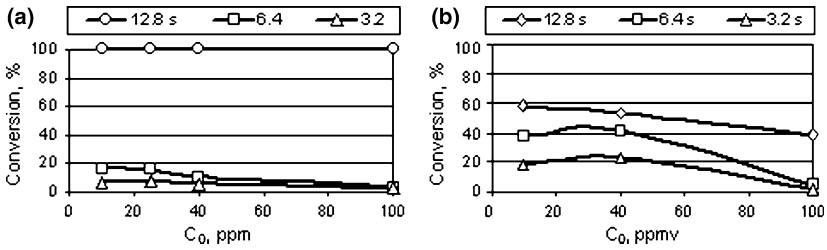

Fig. 7 The dependence of AN conversion rate on its initial concentration at different retention times on sulphated (**a**) and plain P25 (**b**): 130 °C, experiment run time 40 min

at the highest conversion degrees achieved in the experiments. Dependent on the AN inlet concentration, the photonic efficiencies reached the highest values of 3.0 and 0.9% for sulphated and plain P25 respectively at AN inlet concentration of 100 ppm. The lowest corresponding efficiencies at AN inlet concentration of 10 ppm were 0.3 and 0.1%.

The drastic negative effect of temperature decreasing from 130 to 60 °C on AN PCO conversion was observed on sulphated P25 (Fig. 8). The oxidation reaction rates usually depend on temperature increasing with the temperature growth. At the same time adsorption is deteriorated with the temperature increase, compensating the reaction rate improvement having PCO reactions often insensitive towards temperature changes as observed previously with AN PCO at P25 [18]. The 'reaction rate-adsorption' balance at sulphated P25 appears to be dramatically negatively influenced by the temperature decrease practically zeroing its performance. This behaviour is sometimes attributed to thermal catalytic reactions. This possibility is supported by the observation of the minor thermal decomposition reaction at 130 °C and the absence of any reaction at 60 °C. Sulphated titanium dioxide was also found to be more active than P25 at elevated over 100 °C temperatures for PCO of acetaldehyde [15, 32]. It was explained by the quicker deactivation of P25 at elevated temperatures. The sites on P25 were considered to be more active than those on sulphated TiO_2 at lower temperatures, having a broader range of activity than those on sulphated P25. Although thermal catalytic reactions are thought to be similar on both P25 and sulphated P25, they poison P25 more rapidly during PCO at

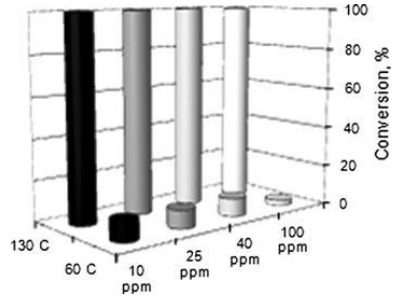

Fig. 8 The conversion of AN with PCO on sulphated P25 at different inlet concentrations and temperatures: retention time 12.8 s, experiment run time 40 min

elevated temperatures, since better adsorption properties of P25 and faster PCO reactions along with AN thermal degradation produce more by-products accumulating on the P25 surface. This explains poor performance of sulphated P25 at lower temperatures.

The gradual improvement of the conversion degree with the increased retention time at Degussa P25 (Fig. 7b) is explained easily with the diminished dilution effect of the gas stream through the reactor and the constant oxidation rate. The disproportional spasmodic increase in conversion at the sulphated catalyst with the retention time increased from 6.3 to 12.8 s at elevated temperature (Fig. 7a), however, may not be simply explained by adsorption properties of the catalyst or the mechanistic increase in the reaction time: the change in the reaction pathway and kinetics is most probably taking place. The AN PCO mechanism through the formation of HNCO intermediate observed

only during PCO on sulphated P25 at maximum residence time studied (12.8 s) could start to prevail and improve the PCO performance, since the gaseous products of HNCO degradation, CO_2 and ammonia, possibly further transform to N_2O (Reaction 3) and easily desorb being seen as gaseous continuous-flow PCO products. This observation is consistent with the PCO performance increased along with experimental run time described earlier: the accumulation of the reaction products at the sulphated TiO_2 possibly catalyzing the conversion at longer retention times may result in the observed sudden increase of the performance.

4 Conclusions

The gaseous product distributions were found to be similar in transient and continuous-flow PCO of AN: CO_2, CO, H_2O and HCN in transient PCO were amended with HNCO and N_2O in continuous-flow mode. The gaseous products of thermal oxidation were CO_2, CO and simplest carbonyl compounds, H_2O, acetonitrile, HCN, NH_3 and trace levels of NO_2. No carbonyl compounds were found after PCO of AN, although the presence of CO among the products shows that they were formed as by-products and further mineralised.

The thermal oxidation with and without simultaneous UV-irradiation after 10-min PCO allowed following the sequence of CN^- group transformation to nitrogen oxides: hydrogen cyanide behaved as an intermediate by-product degrading along with the PCO, which resulted in the accumulation of nitrogen dioxide. The PCO at temperatures about 90 °C allowed complete degrading of intermediate hydrogen cyanide at initial relative concentrations of AN up to 40 ppm.

Sulphated P25 showed better photocatalytic activity at longer retention times and higher temperatures. The AN PCO performance on sulphated P25 was strongly deteriorated at low temperature and shorter retention times.

Acknowledgments The authors express their gratitude to the Estonian Science Foundation (grant 7541 and US16062), and the United States Civilian Research and Development Foundation (grant ESE2-2899-TL-07) for financial support of the research. The help with the transient study equipment at the Department of Chemical and Biological Engineering of the University of Colorado at Boulder (Prof. John L. Falconer and Assoc. Prof. Hans Funke) is greatly appreciated.

References

1. Léonard A, Gerber G, Stecca C, Rueff J, Borba H, Farmer P, Sram R, Czeizel A, Kalina I (1999) Mutat Res 436:263
2. Byrd G, Fowler K, Hicks R, Lovette M, Borgerding M (1990) J Chromatogr 503:359
3. Scherer G, Engl J, Urban M, Gilch G, Janket D, Riedel K (2007) Regul Toxicol Pharm 47:171
4. Huang CC, Lin YC, Lu FC (1999) Separ Sci Technol 34:570
5. Van der Vaart DR, Vatvuk WM, Wehe AH (1991) J Air Waste Manage 41:92
6. Gervasini A, Ragaini V (2000) Catal Today 60:129
7. Hung WC, Chu H (2006) J Environ Eng 132:1482
8. Lu CS, Lin MR, Lin JC (2000) Bioresour Technol 75:35
9. Roach PCJ, Ramsden DK, Hughes J, Williams P (2003) Biotechnol Bioeng 85:450
10. Zhang J, Pierce GE (2009) J Ind Microbiol Biotechnol 36:971
11. Papp J, Soled S, Dwight K, Wold A (1994) Chem Mater 6:496
12. Kozlov D, Paukshtis E, Savinov E (2000) Appl Catal 24:7
13. Arata K (1996) Appl Catal 146:3
14. López T, Bosch P, Tzompantzi F, Gómez R, Navarrete J, López-Salinas E, Llanos ME (2000) Appl Catal 197:107
15. Muggli DS, Ding L, Odland MJ (2002) Catal Lett 78:23
16. Jung SM, Grange P (2000) Catal Lett 76:27
17. Gómez R, López T, Ortiz-Islas E, Navarrete J, Sánchez E, Tzompanztzi F, Bokhimi X (2003) J Mol Catal A 193:217
18. Krichevskaya M, Jõks S, Kachina A, Preis S (2009) Photochem Photobiol Sci 8:600
19. Preis S, Falconer J, del Prado Asensio R, Capdet Santiago N, Kachina A, Kallas J (2006) Appl Catal B 64:79
20. Bayraktar O, Kugler EL (2002) Appl Catal A 233:197
21. Yu HL, Zhang KL, Rossi C (2007) Indoor Built Environ 16:529
22. Larson S, Falconer J (1997) Catal Lett 44:57
23. Miller KL, Lee CW, Falconer J, Medlin J (2010) J Catal. doi: 10.1016/j.jcat.2010.08.011
24. Kozlov D, Bavykin D, Savinov E (2003) Catal Lett 86:196
25. Nanba T, Masukawa S, Uchisawa J, Obuchi A (2008) J Catal 259:250
26. Crowley JN, Sodeau JR (1989) J Phys Chem 93:3100
27. Cant N, Chambers D, Cowan A, Liu I, Satsuma A (2000) Top Catal 10:13
28. Kolinko P, Kozlov D, Vorontsov A, Preis S (2007) Catal Today 122:178
29. Kolinko P, Kozlov D (2009) Appl Catal B 90:126
30. Perez-Ramirez J, Kondratenko E, Kondratenko V, Baerns M (2005) J Catal 229:303
31. Sakthivel S, Shankar MV, Palanichamy M, Arabindoo B, Bahnemann DW, Murugesan V (2004) Water Res 38:3001
32. Muggli DS, Ding L (2001) Appl Catal B 32:181

PAPER III

Jõks, S., Klauson, D., Krichevskaya, M., Preis, S., Qi, F., Weber, A., Moiseev, A., Deubener, J. 2012. Gas-phase photocatalytic activity of nanostructured titanium dioxide from flame aerosol synthesis. - Applied Catalysis B: Environmental, 111-112, p. 1 - 9.

Reprinted with the permission from the Elsevier Limited.
© 2012 Elsevier B.V.

Applied Catalysis B: Environmental 111–112 (2012) 1–9

Contents lists available at SciVerse ScienceDirect

Applied Catalysis B: Environmental

journal homepage: www.elsevier.com/locate/apcatb

Gas-phase photocatalytic activity of nanostructured titanium dioxide from flame aerosol synthesis

Svetlana Jõks[a], Deniss Klauson[a], Marina Krichevskaya[a,*], Sergei Preis[b], Fei Qi[c], Alfred Weber[c], Anna Moiseev[d], Joachim Deubener[d]

[a] Department of Chemical Engineering, Tallinn University of Technology, Ehitajate tee 5, 19086 Tallinn, Estonia
[b] LUT Chemistry, Lappeenranta University of Technology, P.O. Box 20, 53851 Lappeenranta, Finland
[c] Institute of Particle Technology, TU Clausthal, Leibnizstrasse 19, 38678, Clausthal-Zellerfeld, Germany
[d] Institute of Non-Metallic Materials, TU Clausthal, Zehntnerstrasse 2a, 38678, Clausthal-Zellerfeld, Germany

ARTICLE INFO

Article history:
Received 10 June 2011
Received in revised form 5 September 2011
Accepted 9 September 2011
Available online 16 September 2011

Dedicated to Ass. Prof. em. Dr. Eduard Tearo and Ass. Prof. em. Dr. Endel Uus.

Keywords:
Flame aerosol synthesis
Photocatalytic activity
Titanium dioxide
Air pollution
Volatile organic compounds

ABSTRACT

The experimental evaluation of gas-phase photocatalytic activity of a TiO_2 nanopowder synthesized in a flame aerosol reactor was carried out in photocatalytic oxidation (PCO) of volatile organic compounds (VOCs). The nanopowder has an average particle size of 13 nm, anatase content 97 wt.% and the specific surface area of 102 $m^2\ g^{-1}$. The performance was compared to the benchmark photocatalyst, the commercial pyrogenic titania P25, Evonik, with the average particle size of 21 nm. The full-factorial experiments were carried out varying contact times, concentrations of pollutants and temperatures in continuous gas-flow mode degrading aliphatic acrylonitrile (AN) and aromatic toluene. Higher conversions at more stable performance were observed for the flame aerosol synthesized photocatalyst in degradation of both pollutants. While the primary particle size and specific surface area present the apparent reasons for improved PCO performance in adsorbable AN, these parameters cannot do the same in oxidation of poorly adsorbable toluene: the superior generation of hydroxyl radicals and, therefore, advanced oxidative activity are proposed as explanation. The intense dehydration of reduced size anatase crystallites at elevated temperature (130 °C) presumably resulted in decreased OH-radicals production along with the improved desorption of HCN, the PCO by-product of AN. The safe performance is thus requiring lower operational temperatures. Slower deactivation and faster restoration of catalytic activity of flame aerosol synthesized catalyst under UV-A-radiation are discussed.

© 2011 Elsevier B.V. All rights reserved.

1. Introduction

Volatile organic compounds (VOCs) are common air pollutants emitted by chemical, petrochemical, pharmaceutical, and food processing industries, pulp and paper mills, and printing and painting works [1]. VOCs catalytic control technologies could be classified dependently on the pollutants' concentration levels and contaminated air flow rates [2]. Catalytic incineration and combustion techniques require as high as hundreds of ppm concentrations of VOCs and high temperatures (250–1200 °C) for successful operation being cost-ineffective for low pollutant concentrations [3–5]. Low concentrations of VOCs are mostly treated by adsorption and biological oxidation, as well as by non-thermal plasma [2,6]. Photocatalytic oxidation (PCO) technique is of extensive interest recently as potential air-cleaning technology for lower VOCs concentrations and indoor applications [7]. PCO usually uses a near UV-irradiated TiO_2 semiconductor catalyst: the method has oxidation potential sufficient to oxidize the widest spectrum of pollutants at near-ambient temperature [8–10], and is also capable of microbial contamination control of indoor air [11,12]. However, the efficiency of PCO in pollution abatement seems to depend on the chemical nature of the pollutant molecule [13]: catalyst deactivation by oxidation products is the main problem in PCO of, for example, aromatic compounds, trichloroethylene, sulphur- and silicon-containing compounds and others [14–16].Commercial pyrogenic titanium dioxide P25 (Evonik) formed in oxy-hydrogen flame is routinely used as a benchmark photocatalyst in oxidation of VOCs due to its unselective fairly good photoactivity towards wide spectra of pollutants, commercial availability and low cost. However, since the PCO of many organic vapours on P25 is not sufficiently fast for commercial process implementation and the photocatalyst is often deactivated, more active catalysts should be developed. Among various methods, the flame aerosol synthesis of nanopowders is favourable technique for controlling

* Corresponding author. Tel.: +372 6202850; fax: +372 6202856.
E-mail addresses: lanka@starline.ee (S. Jõks), deniss.klauson@ttu.ee (D. Klauson), marina.kritsevskaja@ttu.ee (M. Krichevskaya), sergei.preis@lut.fi (S. Preis), fei.qi@mvt.tu-clausthal.de (F. Qi), weber@mvt.tu-clausthal.de (A. Weber), anna.moiseev@tu-clausthal.de (A. Moiseev), joachim.deubener@tu-clausthal.de (J. Deubener).

0926-3373/$ – see front matter © 2011 Elsevier B.V. All rights reserved.
doi:10.1016/j.apcatb.2011.09.007

crystal structure, particle size and its distribution, thus resulting in generation of open-structure agglomerates [17–21] with catalytic performance exceeding commercial photocatalyst P25 in degradation of aliphatic dichloroacetic acid (DCA) and aromatic 4-chlorophenol (4-CP) in aqueous solutions [22]. The size and crystal phase composition of TiO_2 nanoparticles have been shown crucial for their activity in aqueous phase [23]. However, the lower hydration of catalyst surface in gas-phase PCO brings forward the process sensitivity to the pollutants adsorption–desorption and surface characteristics inducing the difference in photocatalytic activity with aqueous phase. The data on the efficiency of flame synthesized TiO_2 catalysts in air treatment, however, are scarce, only the degradation of acetaldehyde and methanol in batch reactor was described by Balázs et al. [24] using relatively coarse (over 50 nm) anatase nanoparticles from flame synthesis. The improved PCO efficiency in aqueous phenol removal was attributed to the increase in the polyhedral-to-spherical particles ratio, although no improvement was seen in VOCs oxidation in air. To assure the photocatalytic activity of the newly synthesized material exceeding the one of commercially available materials, the gas-phase tests are necessary.

The continuous gas-flow mode used in present research allows following the adsorption/desorption equilibrium of initial pollutants and PCO products, as well as higher concentrations of pollutants could ascertain the deactivation limits of tested photocatalytic materials. Hazardous air pollutants aromatic hydrophobic toluene and aliphatic heteroatomic acrylonitrile (AN) were chosen for gas-phase performance studies of one of the photocatalyst samples F3 synthesized by Moiseev et al. [22] in comparison with commercial P25. AN is detected as an in-door air component emitted by commercial fibrous polymeric materials, resins and smoking tobacco [25,26]; it can induce gene mutations, chromosome aberrations, unscheduled DNA synthesis and cell transformation [27]. Toluene is used as admixture to motor fuel improving octane ratings and also in the synthesis of various organic chemicals and pharmaceuticals, in the production of polymers and as a solvent in paints, coatings, synthetic fragrances, adhesives, inks and cleaning agents [28]. The central nervous system, kidneys, liver and heart are the primary targets for toluene toxicity [29].

The PCO of toluene using commercial TiO_2 catalysts has been extensively studied [30–32]. Regardless of some discrepancies in the PCO products composition, benzoic acid and benzaldehyde intermediates were found to be the products deactivating the photocatalyst [33–35]. Thus, the rate-limiting stage for toluene complete oxidation is PCO of adsorbed intermediates, the degradation rates of which are slower than the one of the parent compound [14,36]. Toluene presents serious problem in the long-term photocatalyst activity exhibiting pronounced deactivation properties [7,37]. The abundance in published data allows toluene being a reference pollutant in characterization of the catalysts and the abatement methods in general. PCO of AN vapours was less studied, the results of P25 and sulphated TiO_2 application were described in recent publications [38,39].

The objective of present paper was to evaluate the gas-phase photocatalytic activity of the new flame synthesized F3 nanopowder photocatalyst compared to commercial P25: the experiments were carried out varying the pollutant concentration, residence time and temperature following the deactivation issues.

2. Experimental

2.1. Materials and analyses

Acrylonitrile (purity ≥ 99.5%, Sigma–Aldrich) and toluene (purity ≥ 99.5%, Lach-Ner) were used as the test air pollutants.

Pyrogenic photocatalyst Aeroxide TiO_2 P25 from Aerosil® process was kindly donated by Evonik Industries (Hanau, Germany) [40–42]. The photocatalyst material labelled F3 used in this study was synthesized as described in [22]: the vapour of the catalyst precursor titanium tetrachloride was formed by passing dry argon gas through a bubbler submerged to the $TiCl_4$-liquid at room temperature. Methane, oxygen and nitrogen were premixed with Ar/$TiCl_4$ and the mixture was introduced into the burner. The flame temperature during synthesis was about 900 °C. The TiO_2 particles were collected on a glass fibre filter placed about 50 cm above the flame. The overall synthesis reaction is given in Eq. (1):

$$TiCl_4(g) + 4O_2(g) + 2CH_4(g) \rightarrow TiO_2(s) + 4HCl(g) + 2CO_2(g) + 2H_2O(g) \quad (1)$$

The feed flow rate of Ar/$TiCl_4$ was varied between 5 and 60 L h^{-1} with the synthesized TiO_2 samples labelled from F1 to F6 in ascendant row of manufacturing rate. The PCO activity of the photocatalyst materials was studied with the aqueous solutions of DCA and 4-CP (see Section 1) ranking the materials in the ascendant order: P25 < F6 < F5 < F4 < **F3** ≅ F1 ≅ F2 [22]. F3 produced at 12 L h^{-1} of Ar/$TiCl_4$ feed rate was selected for gas-phase PCO study as the one with high photocatalytic activity.

The specific surface area of titania powders was determined from the five-point nitrogen adsorption isotherm obtained from Brunauer–Emmett–Teller (BET) measurements using the Gemini 2360 Surface Area Analyzer (Micromeritics, USA). Transmission electron microscopy (TEM) micrographs were obtained with the JEM-2100 microscope (JEOL) operating at 120 kV. The average primary particle size d_{TEM} was estimated as of more than 300 particles. The crystalline phase composition was analysed by X-ray diffraction (XRD) using a Siemens D5000 Kristalloflex instrument and scanning the 2θ range from 15 to 70° at the increment of 0.04°. The relative weight fraction of rutile was determined using Rietveld full-profile refinement with Topas R Software.

Diffuse reflection spectra of P25 and F3 were obtained on a UV-Vis-NIR spectrophotometer Perkin-Elmer Lambda 950, equipped with 150 mm integrating sphere, using Spectralon® as white reference. Simultaneous thermal gravimetric (TG) and differential thermal gravimetric (DTG) analyses were performed on Netsch STA 409 PC Luxx thermal analyzer (TG resolution 2 μg) coupled with mass spectrometer (MS) gas analysis system QMS 403C Aeolos; 100 mg of photocatalyst material was heated in Al_2O_3 crucible with a heating rate of 10 K min^{-1} under nitrogen gas conditions (flow rate of 1 mL min^{-1}).

2.2. Preparation of TiO_2 coating

For photocatalytic experiments the photocatalyst material was fixed to the inner walls of the reactor; the surface of the lamp was free from the catalyst. The coating was formed by the 10-wt.% TiO_2 slurry in distilled water mechanically stirred overnight. The reactor vessel was repeatedly rinsed with TiO_2 slurry with each rinse followed by drying at 120 °C for 2 h. The weighted TiO_2 coating mass of 0.9 g corresponded to the catalyst loading of 1.2 mg TiO_2 per cm^2 of irradiated reactor surface. The roughness of both suspension coatings measured by means of surface profiler TENCOR P-10 was in the range of 1 μm.

Field emission scanning electron microscopy (FE SEM, Dual-Beam Helios Nanolab 600, FEI) was performed to visualize the catalyst coating.

2.3. Photocatalytic tests

Gas-phase photocatalytic experimental equipment was described in detail by Krichevskaya and Preis [36]. The

experimental equipment consists of a thermostatted reactor, gas flow controllers and INTERSPEC 200-X FTIR spectrometer with the Specac Tornado 8-m 1.33-L gas cell with ZnSe-windows. Annular lamp-in-pipe borosilicate glass reactor with total volume of 0.191 L was operated in continuous gas-flow mode. The reactor was composed of an inner glass tube (35 mm outer diameter) and an outer glass tube (45 mm inner diameter, 305 mm length).

A 15 W fluorescent lamp (Philips) with UV-A intensity of 5 mW cm^{-2} was positioned coaxially in the reactor. The UV-A irradiance passing the TiO_2-coating to the reactor's annular clearance space was measured with the UVX Radiometer (Micropulse Technology) and averaged 0.46 for the F3 and 0.15 mW cm^{-2} for P25. No UV-A radiation was detected outside the reactor, *i.e.* no UV-A radiation passed through the double coating of titania.

The VOC feed tank was charged with polluted air by tank evacuation and injection of appropriate model pollutant through the injection port. After 15 min of evaporation, the tank was pressurised with compressed air to 3 bar and left for the concentration balancing overnight. The polluted air stream was diluted with the carrier gas, dry air. The gas flow controllers provided gas flow rates from 0.5 to 4.0 L min^{-1} resulting in pollutant residence time in the reactor from 3 to 23 s. The runs lasted for 60 min with the continuous FT-IR outlet gas analysis.

The temperature in the reactor was maintained at 60 or 130 °C controlled by the heat of the lamp, reactor's insulation and heating tape with the temperature controller (Omega CN9000A).

At the end of each run, the photoreactor with UV lamp and air flow remained turned on was heated up to 180 °C for 3 h after the experiments with AN and for 15 h with toluene to restore the photocatalyst activity. The catalyst's dark adsorption and reproducible PCO activity in subsequently repeated experimental runs were considered as criteria of the catalysts restoration, which practically coincided with the restored white colour of photocatalysts.

Photocatalytic reaction of acrylonitrile and toluene was studied in pollutants' concentration range from 10 to 100 ppm. The AN peaks at the IR bands from 840 to 1100 cm^{-1} and toluene peaks at the IR bands from 700 to 750 and from 2850 to 3130 cm^{-1} were quantified with the detection limit of 1 ppm. The AN and toluene PCO gas-phase products, *i.e.* nitrogen and carbon oxides, water and hydrogen cyanide, were monitored qualitatively and their amounts were relatively compared in arbitrary units by means of FT-IR outlet gas analysis.

Table 1
Characteristics of TiO_2 powders.

TiO_2	BET, m^2 g^{-1}	Average particle size d_{BET}, nm	Average particle size d_{TEM}, nm	Rutile fraction, wt.%
P25	52	29	21	13
F3	102	15	13	3.4

3. Results

3.1. Characterization of photocatalytic materials and coatings

The characteristics of both powders are shown in Table 1. Primary particles of P25 and F3 powders and their agglomerates are shown in Fig. 1.

The morphology of flame aerosol synthesised F3 is similar to that of the commercial product P25: the individual titania particles are linked together in chains forming agglomerates of a few hundred nanometres. The primary particles of both materials are of cubic or polyhedral structure. The calculated average particle size of F3, however, is considerably smaller than that of P25 with d_{TEM} of 13 nm and 21 nm respectively. The flame synthesised titania is as a rule non-porous [20,21]: the d_{BET} (15 nm) of F3 is in good agreement with d_{TEM} (13 nm), whereas d_{BET} of P25 (29 nm) is considerably bigger than d_{TEM} (21 nm) due to higher degree of agglomeration of commercial product.

The primary particle size distributions and diffuse reflectance spectra of P25 and F3 photocatalysts are compared in Fig. 2. The primary particle size distributions of both materials, as determined

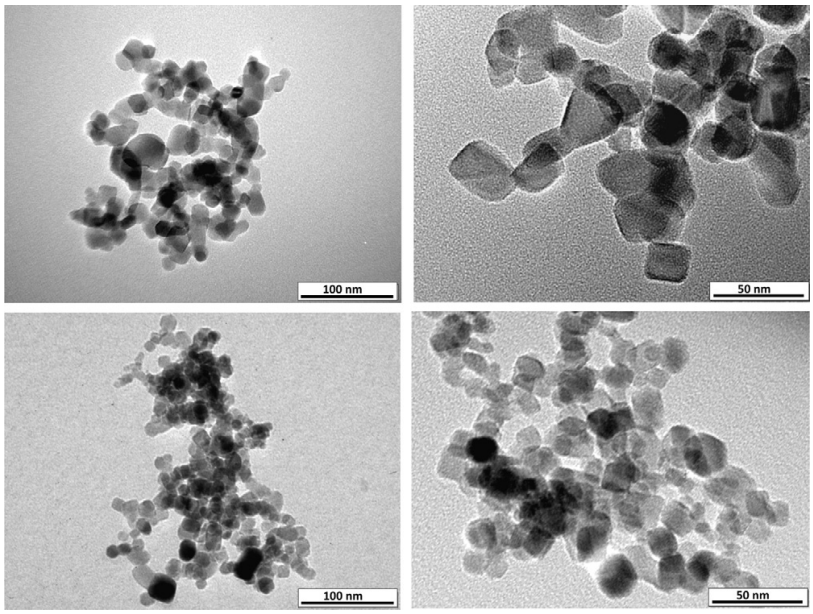

Fig. 1. TEM-images of pyrogenic TiO_2 powders: P25, upper; F3, lower.

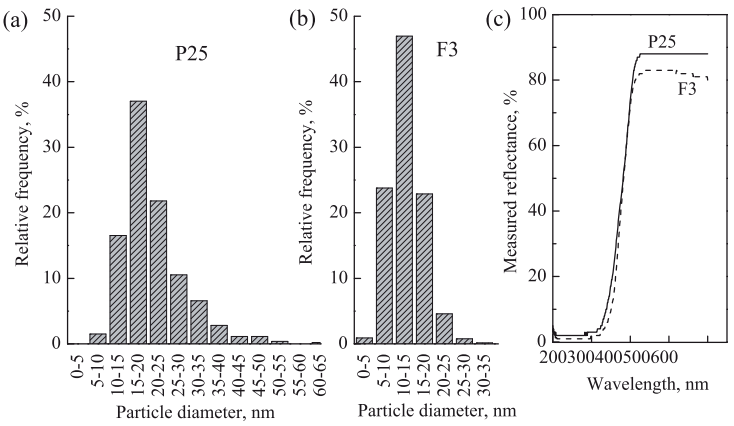

Fig. 2. Primary particle size distribution (a and b) and reflectance spectra (c) of P25 and F3 powders.

from TEM micrographs, are monomodal with a maximum frequency value for a particle size of 15–20 nm and 10–15 nm for P25 and F3 respectively. The diffuse reflectance spectra of P25 and F3 powders have shown no discrepancies in UV-A range. The higher reflectance of P25 in the range between 400 and 600 nm is caused by its higher agglomeration degree.

Although the primary particle size of P25 averages around 21 nm, there is a substantial coarse (about 6% of 35–70 nm) fraction. The inclusions of large crystallites could be also viewed in the agglomerate photo (Fig. 1). The primary particle size distribution of F3 is narrower compared to P25 and contains noticeable fraction, about 25%, of particles sized below 10 nm. The fraction sized above 35 nm is practically absent. However, no "blue" shift in absorption edge of F3 in the range between 300 and 400 nm was observed.

The results of P25 and F3 TG analysis in conjunction with MS (Fig. 3) show the mass loss and the rate of desorption (DTG) of adsorbed water. The DTG and the mass loss were about three times higher for F3 powder at 130 °C, the highest PCO temperature studied, compared to P25, although the difference in specific surface of photocatalytic materials is about the factor of two (Table 1). The considerable water desorption started at temperatures over 50 °C and was still observed at temperatures over 200 °C. The mass loss at 222 °C (filled symbols) achieved 0.75% and 1.85% for P25 and F3 respectively. The broad and intensive peak of appropriate

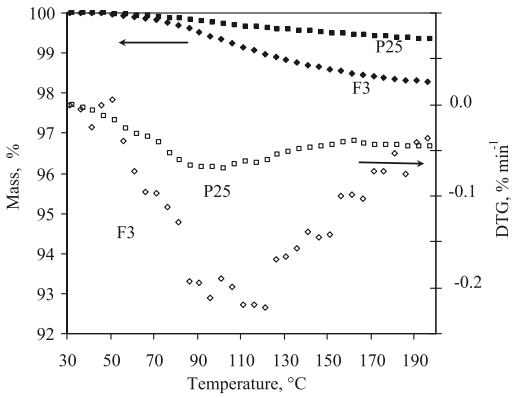

Fig. 3. Thermal analysis profiles of P25 and F3 powders: TG, filled symbols; DTG, open symbols.

DTG curves (open symbols) located at approximately 100 °C was attributed by mass spectrometry to physically adsorbed water. As expected, desorption of bigger quantity of water was observed for F3 having larger surface area.

The SEM images of photocatalyst coatings on borosilicate glass are given in Fig. 4. The individual nanoparticles of photocatalyst materials could be seen in the images with higher resolution. The P25 and F3 coatings show different surface topography and a smoother surface is observed with F3. The difference in agglomeration of TiO_2 particles is apparent in light transmittance through the coating: at equal catalyst coverage, 1.2 mg cm^{-2}, the F3 layer was less opaque and weakens the UV-A intensity about 11 times, whereas P25 coating makes the UV-A light weaker for about 32 times (see Section 2.3). In addition to the F3 less extensive agglomeration, the difference in coatings transparency is also attributed to the plate-like shape of F3 agglomerates different from the spherical one of P25 [22].

3.2. PCO of acrylonitrile

Acrylonitrile at its inlet concentration of 40 ppm at 60 °C and residence time of 23 s was completely adsorbed in the dark on F3 and P25 during the first 40 and 20 min respectively. The difference in adsorption was determined by smaller particles' size and larger contact surface area of F3. After 60 min of experimental run of dark adsorption the concentration of AN in the outlet gas stream comprised about 30% of the AN concentration entered the reactor for both catalysts. At 130 °C the AN adsorption showed similar tendency slightly earlier showing AN in the outlet stream at somewhat smaller adsorbed AN amounts.

The PCO of AN on F3 was examined in the full-factorial experiment at four contact times 3, 6, 11.5 and 23 s, three concentrations 10, 40 and 100 ppm, and two temperatures 60 and 130 °C. The temperature was maintained by working UV-lamp dependent on the insulation of reactor. At 130 °C some aid of the heating tape was applied.

No AN was observed in the outlet of reactor due to its adsorption and conversion ($1-(C_{out}/C_{in})$, %) at 130 °C at all residence times and AN concentrations, as well as at 60 °C at residence times from 11.5 to 23 s over both photocatalysts. The difference in P25 and F3 performance appeared only at 60 °C at residence times of 3 and 6 s with higher AN concentrations, 40 and 100 ppm. The variations in the AN conversion with the residence time of 3 s at 60 °C for both photocatalysts are shown in Fig. 5.

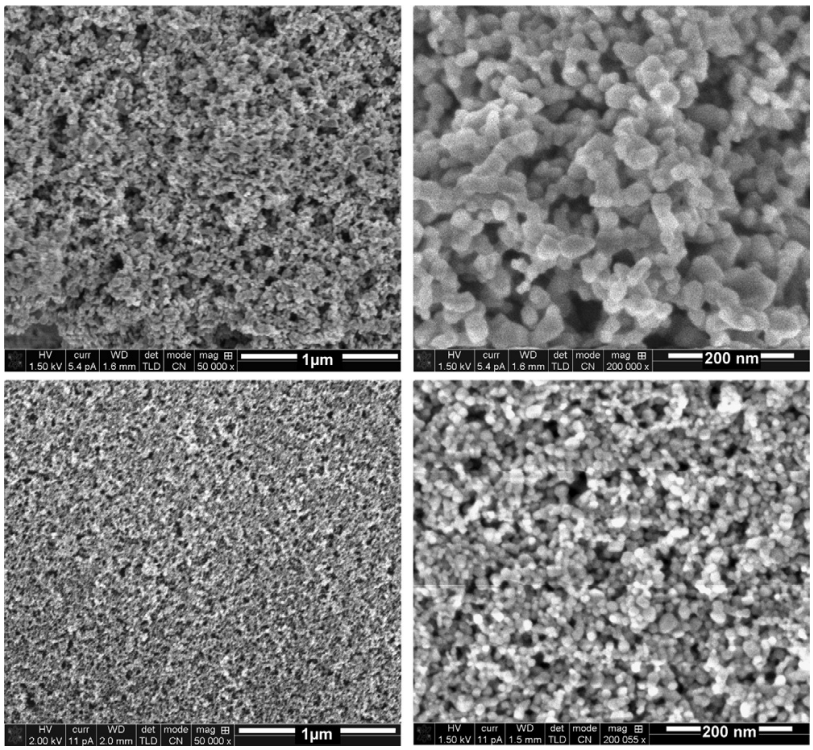

Fig. 4. SEM images of TiO_2 coatings: P25, upper; F3, lower.

From Fig. 5 one can see no AN in the outlet of reactor with F3 coating even at the shortest residence time and high concentrations of AN, whereas deterioration of P25 performance (40 ppm) and even the tendency of its deactivation (100 ppm) were observed.

Besides carbon dioxide and water, the ultimate PCO products, by-products of AN PCO include nitrous oxide, hydrogen cyanide and carbon monoxide in gaseous phase and nitric acid as the product adsorbed on the photocatalyst. The by-products of AN PCO were discussed in detail previously [38,39]. No difference in by-products composition between F3 and P25 was observed.

However, the moment of occurrence of unfavourable HCN within the experimental run time varied for the photocatalysts at 130 °C (see Fig. 6). Hydrogen cyanide did not appear immediately at the starting point of experimental runs, but did in a few minutes; the occurrence of HCN is thus concerned to accumulation of surface-adsorbed reaction products. Hydrogen cyanide was seen to oxidise further to NO_2 forming HNO_3 with water [39]. At 60 °C equal amounts of HCN appear at the same time with both photocatalysts, thus making the overall yield of gaseous hydrogen cyanide per unit of oxidised AN higher for P25, where degradation of AN is incomplete (Fig. 5).

The occurrence of hydrogen cyanide during PCO of AN on the F3 titanium dioxide coating occurred earlier than on P25 mostly at the higher temperature, shorter residence time and lower AN concentrations.

3.3. PCO of toluene

Toluene, being weakly adsorbed on TiO_2 at relatively low temperatures [43], did not adsorb on P25 at 60 and 130 °C. While no adsorption of toluene on F3 was observed at 130 °C, 40% of total toluene amount in the stream containing 40 ppm at residence time

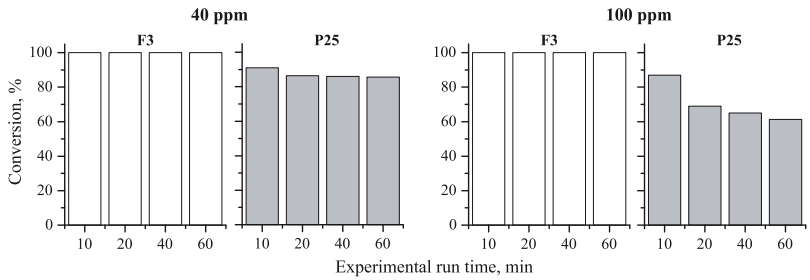

Fig. 5. Acrylonitrile PCO conversion at 60 °C and residence time of 3 s.

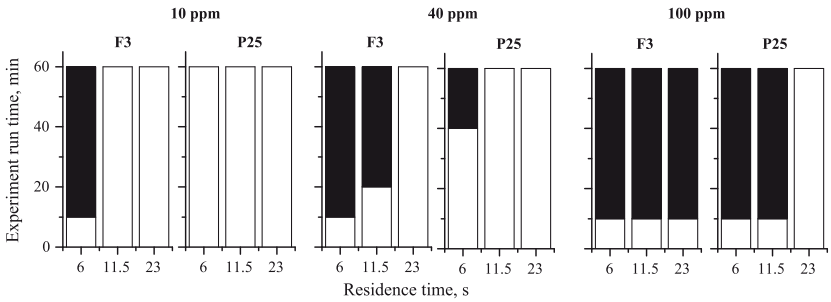

Fig. 6. The occurrence (time, min) of HCN (black columns) during the experimental run with AN at 130 °C.

of 23 s were adsorbed before reaching the adsorption equilibrium at 60 °C, indicating a potential for successful PCO of toluene on F3 photocatalyst.

In the present study toluene expectedly deactivated the photocatalysts. However, at sufficiently low concentration (10 ppm) at residence times from 6 to 23 s at both temperatures no poisoning of both photocatalysts was observed. Moreover, at the longest residence time 23 s no variations in toluene conversion within 60-min run over both catalysts were observed at the toluene initial concentration of 40 ppm at both temperatures, although slight change in photocatalyst colour from white to yellowish indicated possible catalyst deactivation in longer runs. The considerable difference in photocatalysts' performance, however, appeared at shorter residence times of 6 and 11.5 s. Noticeable deterioration in toluene conversion took place at P25 photocatalyst (Fig. 7): at the residence time of 11.5 s the toluene conversion dropped two-fold in 1 h at both temperatures, whereas F3 showed no decline in performance. The F3 photocatalyst showed noticeably slower deactivation in comparison with P25. Earlier photocatalysts deactivation at higher temperature was observed.

There was also noticeable difference in restoration of photocatalyst activity, which was faster for F3 photocatalyst: necessary treatment time to restore the photocatalyst activity and white colour was about 5 h for F3 at the highest toluene concentration and up to 15 h for P25 under identical experimental conditions. This difference could be explained by better UV-light transparency of F3 coating along with its enhanced oxidative ability.

The UV-A radiation passing the TiO_2-coating to the reactor's annular clearance space comprised 9% and 3% for F3 and P25 respectively (see Section 2.3). It could be assumed then that the amount of the UV photons is higher in the intertubular space of F3-reactor allowing its faster restoration.

4. Discussion

The following observations requiring discussion were made:

- higher conversions and stable performance of flame aerosol synthesized F3 photocatalyst towards the degradation of AN and toluene;
- slower deactivation and faster restoration of catalytic activity of F3 catalyst under UV-radiation;
- the earlier, within the experimental run time, appearance of HCN as the AN PCO by-product and, in general, poorer performance of F3 catalyst in HCN abatement at elevated temperatures.

The observations somewhat contradict each other in terms of the new catalyst characterization: the performance of flame aerosol synthesized catalyst substantially improved in toluene and AN oxidation, occurs to be accompanied with enhanced emission of undesired AN PCO by-product hydrogen cyanide, which, although noticed only at the elevated temperature and thus possibly avoided, reveals limitations earlier unknown for the photocatalysts development.

4.1. Improved photocatalytic performance

The improved F3 unselective PCO performance towards well-adsorbed AN and weakly adsorbed toluene indicates the higher oxidative ability of F3 photocatalyst, achieved due to F3 titanium dioxide particle size, increased TiO_2-surface area exposed to irradiation, structural properties and, therefore, superior oxidative ability. The superior character of flame aerosol synthesized catalyst over the benchmark P25 is thus confirmed for the gas-phase PCO similar to the observed in aqueous reactions: both well-adsorbed aliphatic DCA (aq.) and AN (gas), and weakly adsorbed 4-CP (aq.) and toluene (gas) yielded better to PCO at the flame aerosol catalyst [22].

One of the apparent reasons for the improved photocatalytic ability is the catalyst primary particle size and shape: 13 nm F3 particles at least double the surface of 21 nm P25. The positive impact of the reduced particle size is known: the undesired recombination of photogenerated charge carriers in the volume and at the surface of the particle limiting the photocatalysts' activity [44] is reduced due to the migration time of photogenerated charge carriers proportional to the square of the particle size [45]. The overall number of surface active sites also increases with decreasing particle size resulting in accelerated interfacial charge transfer and, consequently, the increased quantum yield [45,46]. Another reason may concern the increased content of anatase thus making the idea of anatase-rutile synergism in gas-phase PCO requiring more detailed quantification. The decreased particle size and the increased content of anatase, however, not always result in improved photocatalytic properties of the catalysts [47], which makes further research in the catalyst properties needed.

The primary particle size, higher anatase content and lower agglomeration degree present the apparent reasons of improved PCO performance for AN adsorbable at the catalyst's surface. The improved performance in poorly adsorbable toluene oxidation, however, cannot be solely explained by larger adsorbing surface: non-adsorbable VOCs should mostly be oxidized by surface OH-radicals, the yield of which also, but not exclusively, is dependent on the water content at the catalyst surface. The water surface content showed disproportional relation to the photocatalysts' specific surface or saturation time – two-fold increased contact surface of F3 adsorbed three-fold amount of water compared to P25 (see Fig. 3), which may also explain accelerated toluene PCO with F3 at all temperatures studied.

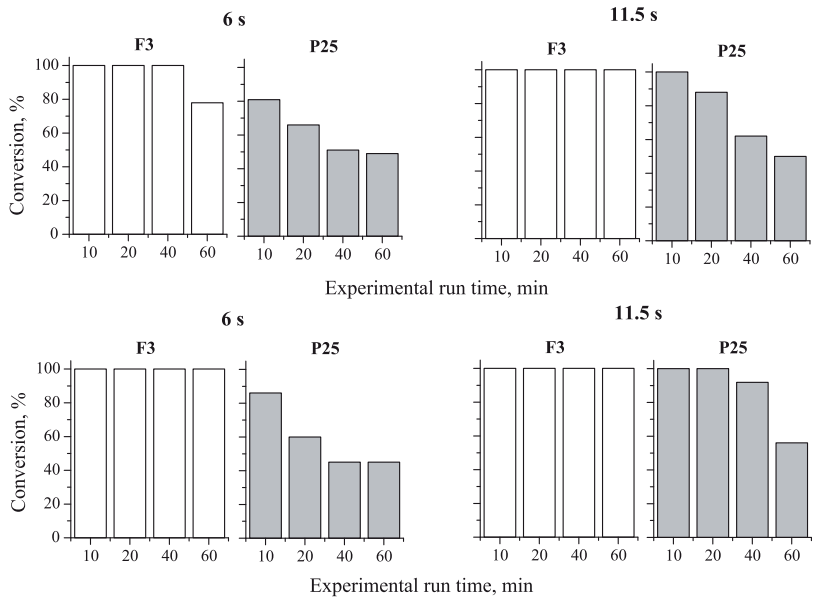

Fig. 7. Toluene PCO conversion at 130 °C (upper) and 60 °C (lower) at inlet concentration of 40 ppm and residence times of 6 and 11.5 s.

4.2. Improved stability

Although there was no decrease in toluene conversion over F3 seen at residence times of 6 and 11.5 s at 60 °C and 11.5 s at 130 °C during the 60-min experimental run, the changes in photocatalyst colour from white to different shades of yellow indicated by-products of toluene oxidation adsorbed on the photocatalyst surface tending towards the catalyst poisoning. At the shortest residence time of 6 s at 130 °C, the photocatalyst deactivation started in 1 h. This could be explained by increased accumulation of toluene PCO intermediates at higher temperatures [48]. This is in an agreement with PCO of toluene on P25, where conversion of toluene dropped from 100 to 60% in 40 min at 130 °C, while it decreased only from 100 to 90% during the same time at 60 °C. No products other than CO_2, CO and H_2O were seen also during the temperature-programmed oxidation after toluene PCO run, where the temperature was raised up to 350 °C, as the main adsorbed PCO by-products also decompose to carbon oxides and water at about this temperature [14].

The recovery of F3 carried out at 180 °C in dry air was accomplished about three times faster than of P25 also indicating stronger photocatalytic potential of the flame aerosol synthesized catalyst. The photocatalytic activity was restored entirely after each of multiple runs.

4.3. Hydrogen cyanide emission

The more incomplete hydrogen cyanide oxidation at elevated temperature with F3 compared to P25 may follow two non-contradictory explanation patterns, the dehydration of the catalyst surface resulted in reduced OH-radicals production at higher temperature (130 °C), and the HCN volatility drastically surpassing the volatility of AN.

Photocatalytic reactions usually are not sensitive to minor variations in temperatures, since the by-product desorption step determines the rate at lower temperatures, whereas the adsorption of reactants is rate determining at higher temperatures [49–51]. When two catalysts with different crystallographic composition and average particle size are compared, the difference in their activity loss at different temperatures is mostly due to their crystallites structure and surface properties. The alteration of photo-production of radicals on heated titanium dioxide was shown by Gonzalez-Elipe et al. [52] and Nakaoka and Nosaka [53]: the change in the radicals' production is caused by the desorption of surface hydroxyl groups and the consequential change in the surface structure. Different reactivity radicals are thus supposed to be formed at different temperatures. The difference in photo-produced radicals at different temperatures could cause the difference in reactivity of the crystallites towards hydrogen cyanide. Bickley and Stone [54] suggested that the loss of adsorbed water would appear to be the main factor governing the decrease in the photoactivity of TiO_2. By measuring the photoadsorption of oxygen and by the quantitative determination of OH groups on the same sample Boonstra and Mutsaers [55] were able to relate these two properties. From the linear relation of oxygen photoadsorption to number of hydroxyl groups after outgassing at different temperatures they concluded that the photoactivity of TiO_2 is determined by the TiOH groups on the surface. It was also found that anatase is more photosensitive to oxygen than rutile. It could be also supposed that anatase crystallites of different sizes possess different sensitivities towards the increased temperature differently loosing the activity due to dehydration. The activity of Pt-group catalysts is also known to be highly sensitive to their particles' size, shape and crystallographic orientation [56–58].

Aqueous photocatalytic oxidation of cyanide was studied earlier and the results may also support the explanation of HCN emission at elevated temperature. The aqueous PCO of cyanide occurs *via* a pure heterogeneous pathway involving the surface hydroxyl groups [59]. The quantum efficiency of the photocatalytic oxidation was found to be low mainly due to the poor adsorption of cyanide ions onto the titanium dioxide surface and, the most important, the absence of homogenous reaction between cyanide ions and diffused hydroxyl radicals.

Table 2
Vapour pressure of selected compounds [61,62].

Compound	Vapour pressure, kPa		
	20 °C	60 °C	130 °C
Toluene	2.9	18.5	170
AN	11.9	57	193[a]
HCN	83	356	1858

[a] At 100 °C.

The gas-phase mechanism of cyanide oxidation is not well-established yet, although the gas-phase and adsorbed products of nitrile group oxidation, N_2O and NO_2 [39], differ greatly from aqueous oxidation products, cyanate and ammonium [59]. Therefore the photocatalyst surface dehydration at 130 °C could be the factor reducing the photocatalytic activity of the catalysts towards cyanide oxidation not significantly hindering the AN oxidation.

Simultaneously, the earlier HCN occurrence on F3 at higher temperature could be attributed to its poor adsorption properties. The different morphology of catalysts result in the rate of water desorption from F3 three-fold exceeding that from P25 indicating poor retention properties of F3 at a higher temperature, also applicable to weakly adsorbed hydrogen cyanide [60]. The HCN high volatility, about six-fold higher than of AN (Table 2) [61,62], also may contribute to the HCN incomplete oxidation at 130 °C. Being extremely unwanted, hydrogen cyanide, however, is easily avoidable under properly selected experimental conditions [39].

5. Conclusions

The superior character of the flame aerosol synthesized catalyst over the commercial P25 titanium dioxide in gas-phase PCO was established for degradation of aliphatic heteroatomic acrylonitrile and aromatic toluene. This supports the unselective character of newly designed catalyst universal for both gaseous and aqueous PCO reactions. The new catalyst surpasses the commercial P25 in, for example, toluene oxidation for over 50% under similar experimental conditions. Slower deactivation and faster complete restoration of catalytic activity of flame synthesized catalyst under UV-A-radiation are also the new catalyst's beneficial key features.

Not only the primary particle size and specific surface area are the reasons for improved PCO performance: the intrinsic materials' properties, such as superior generation of hydroxyl radicals and, therefore, superior oxidative activity may explain the advanced PCO performance with non-adsorbable toluene.

The intense dehydration of the reduced size anatase crystallites in the new catalyst results in decreased OH-radicals production at elevated temperature. Along with the enhanced desorption, this causes a poorer catalyst's performance in PCO of HCN, the PCO product of acrylonitrile. The process safety thus requires lower operational temperatures.

Acknowledgements

The authors express their gratitude to the Estonian Science Foundation (grants 7541 and GUS10), Estonian project SF0140022s10, the United States Civilian Research and Development Foundation (grant ESC2-2974-TL-09) and the Deutsche Forschungsgesellschaft (DFG) (grants DE 598/16-1 and We 2331/10-1) for financial support of the research.

References

[1] R.R. Eldon, D.V.S. Murthy, T. Swaminathan, Process Biochem. 40 (2005) 2771–2779.
[2] S. Revah, J.M. Morgan-Sagastume, in: Z. Shareefdeen, A. Singh (Eds.), Biotechnology for Odor and Air Pollution Control, Springer, Berlin/Heidelberg, 2005, pp. 29–63.
[3] D.R. van der Vaart, W.M. Vatvuk, A.H. Wehe, J. Air Waste Manage. Assoc. 41 (1991) 92–98.
[4] A. Gervasini, V. Ragaini, Catal. Today 60 (2000) 129–138.
[5] W.C. Hung, H. Chu, J. Environ. Eng. 132 (2006) 1482–1488.
[6] K. Hirota, H. Sakai, M. Washio, T. Kojima, Ind. Eng. Chem. Res. 43 (2004) 1185–1191.
[7] Y. Paz, Appl. Catal. B 99 (2010) 448–460.
[8] D.M. Blake, Bibliography of Work on the Heterogeneous Photocatalytic Removal of Hazardous Compounds from Water and Air, Report, National Renewable Energy Laboratory (NREL), Golden, USA, 1995.
[9] D.T. Tompkins, Evaluation of photocatalytic air cleaning capability: a literature review and engineering analysis, ASHARE Research Project RP-1134, 2001.
[10] J. Zhao, X. Yang, Build. Environ. 38 (2003) 645–654.
[11] D.Y. Goswami, D.M. Trivedi, S.S. Block, J. Sol. Energy Eng. 119 (1997) 92–96.
[12] F. Chen, X. Yang, H.K.C. Mak, D.W.T. Chan, Build. Environ. 45 (2010) 1747–1754.
[13] A.J. Maira, K.L. Yeung, J. Soria, J.M. Coronado, C. Belver, C.Y. Lee, V. Augugliaro, Appl. Catal. B 29 (2001) 327–336.
[14] S.A. Larson, J.L. Falconer, Catal. Lett. 44 (1997) 57–65.
[15] D.F. Ollis, CR Acad. Sci. II C 3 (2000) 405–411.
[16] S.O. Hay, T.N. Obee, C. Thibaud-Erkey, Appl. Catal. B 99 (2010) 435–441.
[17] G.D. Ulrich, Chem. Eng. News 6 (1984) 22–29.
[18] S.E. Pratsinis, Prog. Energy Combust. Sci. 24 (1998) 197–219.
[19] W.J. Stark, S.E. Pratsinis, Powder Technol. 126 (2002) 103–108.
[20] R. Strobel, W.J. Stark, L. Mädler, S.E. Pratsinis, A. Baiker, J. Catal. 213 (2003) 296–304.
[21] R. Strobel, A. Baiker, S.E. Pratsinis, Adv. Powder Technol. 17 (2006) 457–480.
[22] A. Moiseev, F. Qi, J. Deubener, A. Weber, Chem. Eng. J. 170 (2011) 308–315.
[23] Z. Zhang, C.-C. Wang, R. Zakaria, J.Y. Ying, J. Phys. Chem. B 102 (1998) 10871–10878.
[24] N. Balázs, A. Gácsi, A. Pallagi, K. Mogyorósi, T. Alapi, P. Sipos, A. Dombi, React. Kinet. Mech. Catal. 102 (2011) 283–294.
[25] G. Byrd, K. Fowler, R. Hicks, M. Lovette, M. Borgerding, J. Chromatogr. A 503 (1990) 359–436.
[26] G. Scherer, J. Engl, M. Urban, G. Gilch, D. Janket, K. Riedel, Regul. Toxicol. Pharmacol. 47 (2007) 171–183.
[27] A. Léonard, G.B. Gerber, C. Stecca, J. Rueff, H. Borba, P.B. Farmer, R.J. Sram, A.J. Czeizel, I. Kalina, Mutat. Res. 436 (1999) 263–283.
[28] EPA – Environmental Protection Agency, Integrated Risk Information System (IRIS) on Toluene, National Center for Environmental Assessment, Office of Research and Development, Washington, 1999.
[29] ATSDR – Agency for Toxic Substances and Disease Registry, Toxicological Profile for Toluene, U.S. Public Health Service, U.S. Department of Health and Human Services, Atlanta, 1994.
[30] T. Ibusuki, K. Takeuchi, Atmos. Environ. 20 (1967) 1711–1715.
[31] R. Méndez-Román, N. Cardona-Martínez, Catal. Today 40 (1998) 353–365.
[32] V. Augugliaro, S. Coluccia, V. Loddo, L. Marchese, G. Martra, L. Palmisano, M. Schiavello, Appl. Catal. B 20 (1999) 15–27.
[33] E. Piera, J.A. Ayllon, X. Domenech, J. Peral, Catal. Today 76 (2002) 259–270.
[34] C. Belver, M.J. Lopez-Munoz, J.M. Coronado, J. Soria, Appl. Catal. B 46 (2003) 497–509.
[35] J. Mo, Y. Zhang, Q. Xu, J. Joaquin Lamson, R. Zhao, Atmos. Environ. 43 (2009) 2229–2246.
[36] M. Krichevskaya, S. Preis, J. Adv. Oxid. Technol. 6 (2003) 150–157.
[37] T.N. Obee, R.T. Brown, Environ. Sci. Technol. 29 (1995) 1223–1231.
[38] M. Krichevskaya, S. Jõks, A. Kachina, S. Preis, Photochem. Photobiol. Sci. 8 (2009) 600–603.
[39] S. Jõks, M. Krichevskaya, S. Preis, Catal. Lett. 141 (2011) 309–315.
[40] Titanium Dioxide P25—Manufacture—Properties—Applications, Technical Bulletin Fine Particles, Evonik Degussa Corp., Number 80, 2003.
[41] Basic Characteristics of Aerosil, Technical Bulletin Fine Particles, Evonik Degussa Corp., Number 11, 2006.
[42] C. Schulze Istfort, M. Rochnia, Toxicol. Lett. 186 (2009) 148–151.
[43] M.C. Blount, J.L. Falconer, J. Catal. 200 (2001) 21–33.
[44] C.-Y. Wang, J. Rabani, D.W. Bahnemann, J.K. Dohrmann, J. Photochem. Photobiol. A 148 (2002) 169–176.
[45] A.R. Kortan, R. Hull, R.L. Opila, M.G. Bawendi, M.L. Steigerwald, P.J. Carroll, L.E. Brus, J. Am. Chem. Soc. 112 (1990) 1327–1332.
[46] N. Serpone, D. Lawless, R. Khairutdinov, E. Pelizzetti, J. Phys. Chem. 99 (1995) 16655–16661.
[47] G.P. Fotou, S.E. Pratsinis, Chem. Eng. Commun. 151 (1996) 251–269.
[48] T. Guo, Z. Bai, C. Wu, T. Zhu, Front. Environ. Sci. Eng. China 2 (2008) 224–229.
[49] P. Pichat, J.M. Hermann, in: N. Serpone, E. Pelizzetti (Eds.), Photocatalysis: Fundamentals and Applications, John Wiley & Sons, NTC, 1989, pp. 217–250.
[50] M.A. Fox, M.T. Dulay, Chem. Rev. 93 (1993) 341–357.
[51] S.B. Kim, H.T. Hwang, S.C. Hong, Chemosphere 48 (2002) 437–444.
[52] A.R. Gonzalez-Elipe, G. Munuera, J. Soria, J. Chem. Soc. Faraday Trans. I 75 (1979) 748–761.
[53] Y. Nakaoka, Y. Nosaka, J. Photochem. Photobiol. A 110 (1997) 299–305.
[54] R.I. Bickley, F.S. Stone, J. Catal. 31 (1973) 389–397.
[55] A.H. Boonstra, C.A.H.A. Mutsaers, J. Phys. Chem. 79 (1975) 1694–1698.
[56] N. Tian, Z.-Y. Zhou, S.-G. Sun, Y. Ding, Z.L. Wang, Science 316 (2007) 732–735.
[57] V. Komanicky, H. Iddir, K.-C. Chang, A. Menzel, G. Karapetrov, D.C. Hennessy, P. Zapol, H. You, Electrochim. Acta 55 (2010) 7934–7938.

[58] B. Roldan Cuenya, Thin Solid Films 518 (2010) 3127–3150.
[59] K. Chiang, R. Amal, T. Tran, J. Mol. Catal. A: Chem. 193 (2003) 285–297.
[60] C.H. Pollema, J.L. Hendrix, E.B. Milosavljevic, L. Solujic, J.H. Nelson, J. Photochem. Photobiol. A 66 (1992) 235–242.
[61] T.E. Jordan, Vapor Pressure of Organic Compounds, Interscience Publishers Inc., New York, 1954.
[62] H.G. Hirschenberg, Verfahrenstechnik und Anlagenblau: Chemie, Technik, Wirtschaftlichkeit, Springer, Berlin, 1999.

APPENDIX II. CURRICULUM VITAE

ELULOOKIRJELDUS

1. Isikuandmed

Ees- ja perekonnanimi: Svetlana Jõks
Sünniaeg ja –koht: 29. november 1982.a., Tapa
Kodakondsus: eesti

2. Kontaktandmed

Aadress: TTÜ, Keemiatehnika instutuut, Ehitajate tee 5, 19086 Tallinn, Eesti
Telefon: +372 620 2850
E-posti aadress: svetlana@present.ee

3. Hariduskäik

Õppeasutus (nimetus lõpetamise ajal)	Lõpetamise aeg	Haridus (eriala/kraad)
Tallinna Tehnikaülikool	2008	Tehnikateaduste magistrikraad
Tallinna Tehnikaülikool	2005	Tehnikateaduste bakalaureusekraad
Tapa Vene Gümnaasium	2002	Keskharidus

4. Keelteoskus (alg-, kesk- või kõrgtase)

Keel	Tase
Eesti	Kõrgtase
Vene	Kõrgtase
Inglise	Kesktase

5. Täiendusõpe

Õppimise aeg	Täiendusõppe läbiviija nimetus
2010 - 2010	Colorado Ülikool, USA

6. Teenistuskäik

Töötamise aeg	Tööandja nimetus	Ametikoht
2011-k.a.	JS Keemia AS	müügijuht
2008-2008	TTÜ	laborant

7. Teadustegevus:

Akrüülnitriili fotokatalüütiline oksüdatsioon gaasifaasis (2008-2010).

Akrüülnitriili fotokatalüütiline oksüdatsioon gaasifaasis sulfateeritud katalüsaatoriga pideva töörežiimiga torureaktoris ning poolperioodilises reaktoris kasutades temperatuur-programmeeritud oksüdatsiooni meetodit (2009-2010).

Leekaerosoolmeetodiga sünteesitud titaaniumdioksiidi fotokatalüütiline aktiivsus gaasifaasis (2010-2011).

8. Kaitstud lõputööd:

Tehnikateaduste magistrikraad (2008): Akrüülnitriili fotokatalüütiline oksüdatsioon gaasifaasis. Juhendaja: Keemiatehnika instituudi vanemteadur Marina Kritševskaja

9. Teadustöö põhisuunad:

Gaasiliste orgaaniliste saasteainete fotokatalüütiline oksüdatsioon. Fotokatalüütilise oksüdatsiooni lendavate produktide kvalitatiivne määramine FTIR-spektroskoopia abil.

10. Teised uurimisprojektid

Projekt ETF8978 (2012 – k.a.): Toksiliste keskkonnaohtlike ainete lagundamine vees fotokatalüüsi ja bioloogilise oksüdatsiooni kombineerimisel ning õhus fotokatalüüsiga

Projekt GUS10 (2010 – k.a.): Fotokatalüüsi kombinatsioon fermentatsiooniga vesilahustest vesiniku ja hapniku tootmiseks

Projekt SF0140022s10 (2010-k.a.): Keemiatehnilised aspektid keskkonnariskide hindamisel

Projekt ETF7541 (2008 – 2010): Nähtavas valguses aktiivsete fotokatalüsaatorite süntees ja nende kinnitamine pindadele saasteainete mineraliseerimiseks

Projekt GUS16062 (2008 – 2009): The development of photocatalysts for the visible light

CURRICULUM VITAE

1. Personal data

Name: Svetlana Jõks
Date and place of birth: 29th November 1982, Tapa

2. Contact information

Address: TUT, department of Chemical Engineering, Ehitajate tee 5, 19086 Tallinn, Estonia
Phone: : +372 620 2850
E-mail: svetlana@present.ee

3. Education

Educational institution	Graduation year	Education (field of study/degree)
Tallinn University of Technology	2008	Master of Science
Tallinn University of Technology	2005	Bachelor of Science
Tapa Vene Gümnaasium	2002	High school education

4. Language competence/skills (fluent; average, basic skills)

Language	Level
Estonian	Fluent
Russian	Fluent
English	Average

5. Special Courses

Period	Educational or organisation
2010-2010	University of Colorado, USA

6. Professional Employment

Period	Organisation	Position
2011-onwards	JS Chemistry LTD	Sales manager
2008-2008	TUT	Laboratory technician

7. Scientific work:

Gas-phase photocatalytic oxidation of acrylonitrile (2008-2010).

Gas-phase photocatalytic oxidation of acrylonitrile on sulphated TiO_2: continuous flow and transient study (2009-2010).

Gas-phase photocatalytic activity of nanostructured titanium dioxide from flame aerosol synthesis (2010-2011).

8. Defended theses:

Msc thesis in Engineering (2008): Gas-phase photocatalytic oxidation of acrylonitrile.
Supervisor: senior researcher Marina Kritševskaja

9. Main areas of scientific work/Current research topics:

Gas-phase photocatalytic oxidation of organic air pollutants. Photocatalytic oxidation products analysis by FTIR spectroscopy.

10. Other research projects:

Project ETF8978 (2012- onwards): Degradation of environmentally toxic refractory compounds in water by combination of photocatalysis and biological treatment and in air by photocatalysis

Project SF0140022s10 (2010- onwards): Chemical Engineering Aspects in Environmental Risk Assessment

Project GUS10 (2010– onwards): Photocatalysis combination with dark fermentation for hydrogen and oxygen production from aqueous solutions

Project ETF7541 (2008–2010): Synthesis of photocatalysts active under visible light and their immobilization on surfaces for mineralisation of environmental pollutants

Project GUS16062 (2008–2009): The development of photocatalysts for the visible light

DISSERTATIONS DEFENDED AT TALLINN UNIVERSITY OF TECHNOLOGY ON CHEMISTRY AND CHEMICAL ENGINEERING

1. **Endel Piiroja**. Oxidation and Destruction of Polyethylene. 1993.

2. **Meili Rei**. Lihatehnoloogia teaduslikud alused. Fundamentals of Food Technology. 1995.

3. **Meeme Põldme**. Phase Transformations in Hydrothermal Sintering Processing of Phosphate Rock. 1995.

4. **Kaia Tõnsuaadu**. Thermophosphates from Kovdor and Siilinjärvi Apatites. 1995.

5. **Anu Hamburg**. The Influence of Food Processing and Storage on the N-Nitrosamines Formation and Content in Some Estonian Foodstuffs. 1995.

6. **Ruth Kuldvee**. Computerized Sampling in Ion Chromatography and in Capillary Electrophoresis. 1999.

7. **Külliki Varvas**. Enzymatic Oxidation of Arachidonic Acid in the Coral Gersemia fruticosa. 1999.

8. **Marina Kudrjašova**. Application of Factor Analysis to Thermochromatography and Promotion Studies. 2000.

9. **Viia Lepane**. Characterization of Aquatic Humic Substances by Size Exclusion Chromatography and Capillary Electrophoresis. 2001.

10. **Andres Trikkel**. Estonian Calcareous Rocks and Oil Shale Ash as Sorbents for SO_2. 2001.

11. **Marina Kritševskaja**. Photocatalytic Oxidation of Organic Pollutants in Aqueous and Gaseous Phases. 2003.

12. **Inna Kamenev**. Aerobic Bio-Oxidation with Ozonation in Recalcitrant Wastewater Treatment. 2003.

13. **Janek Reinik**. Methods for Purification of Xylidine-Polluted Water. 2003.

14. **Andres Krumme**. Crystallisation Behaviour of High Density Polyethylene Blends with Bimodal Molar Mass Distribution. 2003.

15. **Anna Goi**. Advanced Oxidation Processes for Water Purification and Soil Remediation. 2005.

16. **Pille Meier**. Influence of Aqueous Solutions of Organic Substances on Structure and Properties of Pinewood (Pinus sylvestris). 2007.

17. **Kristjan Kruusement**. Water Conversion of Oil Shales and Biomass. 2007.

18. **Niina Kulik**. The Application of Fenton-Based Processes for Wastewater and Soil Treatment. 2008.

19. **Raul Järviste**. The Study of the Changes of Diesel Fuel Properties a its Long Term Storage. 2008.

20. **Mai Uibu**. Abatement of CO2 Emissions in Estonian Oil Shale-Based Power Production. 2008.

21. **Valeri Gorkunov**. Calcium-Aluminothermal Production of Niobium and Utilization of Wastes. 2008.

22. **Elina Portjanskaja**. Photocatalytic Oxidation of Natural Polymers in Aqueous Solutions. 2009.

23. **Karin Reinhold**. Workplace Assessment: Determination of Hazards Profile using a Flexible Risk Assessment Method. 2009.

24. **Natalja Savest**. Solvent Swelling of Estonian Oil Shales: Low Temperature Thermochemical Conversion Caused Changes in Swelling. 2010.

25. **Triin Märtson**. Methodology and Equipment for Optical Studies of Fast Crystallizing Polymers. 2010.

26. **Deniss Klauson**. Aqueous Photocatalytic Oxidation of Non-Biodegradable Pollutants. 2010.

27. **Oliver Järvik**. Intensification of Activated Sludge Process – the Impact of Ozone and Activated Carbon. 2011.

28. **Triinu Poltimäe**. Thermal Analysis of Crystallization Behaviour of Polyethylene Copolymers and Their Blends. 2011.

29. **Mariliis Sihtmäe**. (Eco)toxicological Information on REACH-Relevant Chemicals: Contribution of Alternative Methods to in vivo Approaches. 2011.

30. **Olga Velts**. Oil Shale Ash as a Source of Calcium for Calcium Carbonate: Process Feasibility, Mechanism and Modeling. 2011.